Journal of Medicinal Chemistry

Article

Identification of a Multitargeted Tyrosine Kinase Inhibitor for the Treatment of Gastrointestinal Stromal Tumors (GISTs) and Acute Myeloid Leukemia (AML)

Wen-Hsing Lin, Suying Wu, Teng-Kuang Yeh, Chiung-Tong Chen, Jen-Shin Song, Hui-Yi Shiao, Ching-Chuan Kuo, Tsu Hsu, Cheng-Tai Lu, Pei-Chen Wang, Tsung-Sheng Wu, Yi-Hui Peng, Hui-You Lin, Ching-Ping Chen, Ya-Ling Weng, Fang-Chun Kung, Mine-Hsine Wu, Yu-Chieh Su, Kuo-Wei Huang, Ling-Hui Chou, Ching-Cheng Hsueh, Kuei-Jung Yen, Po-Chu Kuo, Chen-Lung Huang, Li-Tzong Chen, Chuan Shih, Hui-Jen Tsai, and Weir-Torn Jiaang

J. Med. Chem., **Just Accepted Manuscript** • DOI: 10.1021/acs.jmedchem.9b01229 • Publication Date (Web): 13 Nov 2019

is published by the American Chemical Society. 1155 Sixteenth Street N.W., Washington, DC 20036

Identification of a Multitargeted Tyrosine Kinase Inhibitor for the Treatment of Gastrointestinal Stromal Tumors (GISTs) and Acute Myeloid Leukemia (AML)

Wen-Hsing Lin,[1,#] Su-Ying Wu,[1,#] Teng-Kuang Yeh,[1,#] Chiung-Tong Chen,[1] Jen-Shin Song,[1] Hui-Yi Shiao, Ching-Chuan Kuo,[1] Tsu Hsu,[1] Cheng-Tai Lu,[1] Pei-Chen Wang, Tsung-Sheng Wu,[1] Yi-Hui Peng,[1] Hui-You Lin,[2] Ching-Ping Chen,[1] Ya-Ling Weng, Fang-Chun Kung,[1] Mine-Hsine Wu,[1] Yu-Chieh Su,[1] Kuo-Wei Huang,[2] Ling-Hui Chou,[1] Ching-Cheng Hsueh,[1] Kuei-Jung Yen,[1] Po-Chu Kuo,[1] Chen-Lung Huang,[1] Li-Tzong Chen,[2,3,5,6] Chuan Shih,[1] Hui-Jen Tsai,[2,3,4]* and Weir-Torn Jiaang[1,*]

[1]Institute of Biotechnology and Pharmaceutical Research, National Health Research Institutes, No. 35, Keyan Rd., Zhunan Town, Miaoli Country 350, Taiwan R.O.C.

[2]National Institute of Cancer Research, National Health Research Institutes, Tainan City 704, Taiwan R.O.C.

[3]Division of Hematology/Oncology, Department of Internal Medicine, National Cheng Kung University Hospital, College of Medicine, National Cheng Kung University, Tainan City 704, Taiwan R.O.C

[4]Division of Hematology/Oncology, Department of Internal Medicine, Kaohsiung Medical University Hospital, Kaohsiung Medical University, Kaohsiung 807, Taiwan R.O.C.

[5]Institute of Molecular Medicine, National Cheng Kung University, Tainan City 704, Taiwan R.O.C.

[6]Division of Gastroenterology, Department of Internal Medicine, Kaohsiung Medical University Hospital, Kaohsiung Medical University, Kaohsiung 807, Taiwan R.O.C.

[#] Wen-Hsing Lin, Su-Ying Wu, and Teng-Kuang Yeh contributed equally.

*Corresponding authors

Abstract

Gastrointestinal stromal tumors (GISTs) are prototypes of stem cell factor receptor (c-KIT)-driven cancer. Two receptor tyrosine kinases, c-KIT and fms-tyrosine kinase (FLT3), are frequently mutated in AML patients, and these mutations are associated with poor prognosis. In this study, we discovered a multitargeted tyrosine kinase inhibitor, compound **15a**, with potent inhibition against single or double mutations of c-KIT developed in GISTs. Moreover, crystal structure analysis revealed the unique binding mode of **15a** with c-KIT and may elucidate its high potency in inhibiting c-KIT kinase activity. Compound **15a** inhibited cell proliferation and induced apoptosis by targeting c-KIT in c-KIT-mutant GIST cell lines. The antitumor effects of **15a** were also demonstrated in GIST430 and GIST patient-derived xenograft (PDX) models. Further studies demonstrated that **15a** inhibited the proliferation of c-KIT- and FLT3-driven AML cells *in vitro* and *in vivo*. The results of this study suggest that **15a** may be a potential anticancer drug for the treatment of GISTs and AML.

Keywords: Multitargeted tyrosine kinase inhibitor, Gastrointestinal stromal tumors, Acute myeloid leukemia, GIST430, Patient-derived xenograft model

Introduction

Gastrointestinal stromal tumors (GISTs) are mesenchymal neoplasms that develop in the gastrointestinal tract. GISTs are thought to derive from the interstitial cells of Cajal.[1] Worldwide, epidemiological data show that the annual incidence of GISTs is approximately 10−20 cases per million people.[2] These tumors can occur at any site but are predominantly found in the stomach and small intestine.[1] Approximately 60% of patients with operable GISTs can be cured by surgery. However, about 40% of localized GISTs develop metastasis.[1] Unresectable and/or metastatic GISTs have poor responses to conventional chemotherapy and radiation therapy. c-KIT mutations were found in most GISTs and act as a driver gene for GISTs.[3] Understanding the underlying cause of GISTs has led to the development and investigation of new agents targeting c-KIT. These drugs effectively inhibit the activity of mutant forms of c-KIT in tumors and significantly improve the clinical outcomes for patients with advanced GISTs.[4,5] Currently, there are three c-KIT tyrosine kinase inhibitors (TKIs) approved for treatment of advanced GISTs (Figure 1).[5] The standard first-line treatment is imatinib (**1**). Treatment with **1** in advanced GISTs successfully achieved a disease control rate of 81.6% and significantly improved progression-free survival (PFS) and overall survival (OS) in a phase II clinical trial.[6] The results from a phase II and a phase III trial suggest compound **1** achieves a long-term median OS of 51−57 months in patients with advanced or metastatic GISTs.[7,8]

Although compound **1** has good response to GISTs, disease progression or

recurrence still may develop by either primary or secondary resistance to **1**.[9,10] c-KIT mutations have been found in approximately 80% of GISTs. Mutations at exon 9 and exon 11 are the most common primary mutations identified at initial diagnosis of GISTs. Approximately 7% of GISTs have PDGFRα gene mutations.[11,12] GIST patients who are not responsive to first-line **1** treatment within 6 months are classified as primary resistance to **1**. Patients with exon 11 mutations have better response and survival to **1**, whereas those with exon 9 mutations have worse treatment outcomes.[12−14] GIST patients with wild type c-KIT or PDGFRα gene mutations are usually resistant to **1**. Moreover, patients who develop resistance to **1** after 6 months of treatment are classified as secondary resistance and about 50% of these patients develop a secondary mutation in either exon 13, 14, 17 or 18 of c-KIT. The majority of these secondary mutations developed in patents with primary mutations in exon 11 of c-KIT.[15,16] For **1**-resistant GIST patient, sunitinib (**2**), a multitargeted tyrosine kinase inhibitor, was approved as a second-line treatment for advanced GIST patients after failure of compound **1** therapy.[17] In addition, regorafenib (**3**) is another multitargeted tyrosine kinase inhibitor approved in 2013 as the third-line treatment for GIST patients who were resistant or intolerant to **1** and **2**.[18] However, the median PFS achieved by compounds **2** and **3** are only 6.8 and 4.8 months, respectively.[5] Therefore, the development and identification of novel agents for refractory GISTs is urgently required.[5,18]

Acute myeloid leukemia (AML) is a hematologic malignancy with uncontrolled proliferation and impaired maturation of hematopoietic cells. A high percentage of AML

patients relapse despite the apparent success of initial induction chemotherapy. The occurrence of oncogenic mutations that leads to aberrant activation and proliferation of cellular signal transduction pathways results in primary treatment failure in AML and provides insight into the refractory nature of AML.[19] FMS-like tyrosine kinase-3 (FLT3) is a member of the class III membrane-bound receptor tyrosine kinase (RTK) family. In addition to FLT3, RTK class III includes c-KIT, CSF1R (FMS), PDGFRα and PDGFRβ.[20] FLT3 mutations have been identified in approximately 30% of all AML patients and these mutations are indicative of poor prognosis.[21,22] The mutations include internal tandem duplications (ITDs) in the juxtamembrane domain of FLT3 and missense point or short-length mutations in the activation loop (AL) of the tyrosine kinase domain (TKD).[23,24] Notably, c-KIT are mutated in a subset of AML (core-binding factor (CBF)-AML) with a range of 17-46% mutation rate.[25-29] Even though CBF-AML patients usually have longer survival than other poor-risk patients, CBF-AML patients with c-KIT mutation have higher risk of relapse and usually have poor survival, particularly with D816V mutation.[28-30]

Mutations in both FLT3 and c-KIT are significantly associated with poor prognosis in patients with AML, the development of agents that target these mutations has emerged as promising therapeutic strategies for the treatment of AML.[31] Currently, midostaurin (PKC-412, **4**, Figure 1) is the only approved TKI in combination with standard intensive chemotherapy for adult patients with newly diagnosed FLT3-mutated AML. The international phase III trial results indicated that randomized patients to receive compound **4** (Figure 1) had

a higher median OS, with a hazard ratio of 0.78 compared with those receiving placebo.[32] By the end of 2018, the Food and Drug Administration approved gilteritinib for the treatment of adult patients who have relapsed or refractory AML with a FLT3 mutation.[33] The mutation sites of c-KIT in CBF-AML mainly located on exon 8 (D419) and exon 17 (D816 and N822).[34] Several agents targeting c-KIT, such as compound **1** and dasatinib, have been shown to suppress the proliferation of c-KIT mutant leukemia cells *in vitro*.[35,36] Compound **1** failed to respond to relapsed AML patients with c-KIT mutations in earlier study.[37] Recently, dasatinib in combination of intensive chemotherapy was shown to induce a higher response rate for CBF-AML[38] and the phase III trial is still ongoing.

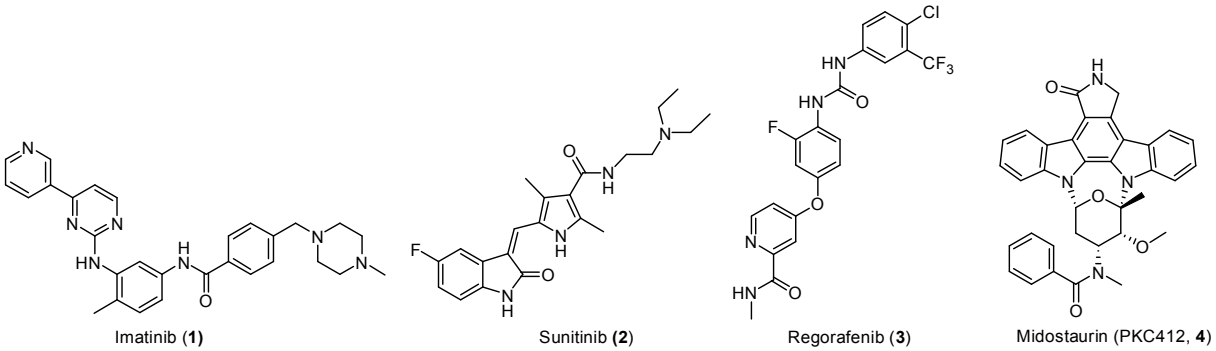

Figure 1. Structures of c-KIT and FLT3 inhibitors in the clinic.

Design of Multitargeted Tyrosine Kinase Inhibitors

Using a structure-based design, we previously developed a novel class of 5-phenylthiazol-2-ylamine-based derivatives (Structure **O,** Figure 2) as a versatile template for the development of multitargeted kinase inhibitors. This previous study led to the

discovery of urea **5**, which exhibited promising *in vitro* and *in vivo* antitumor activities against FLT3-ITD–expressing MOLM-13 and MV4;11 cell lines and FLT3-ITD/D835Y–expressing 32D cell lines.[39] Kinome-wide selectivity profile of **5** with DiscoveRx's KinomeScan technology[40] demonstrated that **5** bore a low selectivity (S score (10) = 0.091 at a low concentration of 0.1 μM) among 395 wild-type kinases tested. Both multikinase inhibitors and single-kinase inhibitors have advantages and disadvantages, which are related to potential resistance mechanisms, pharmacokinetics, selectivity, tumor environment and toxicity.[41] However, we speculate that the off-target profile of **5** might explain its intrinsic toxicity *in vivo*. To trim the off-target profile, optimize target inhibition and increase the therapeutic window with acceptable toxicity, we rationally designed a second class of heteroaryl-substituted 2-aminothiazole derivatives as multikinase inhibitors (Structure **P,** Figure 2). The approach removes an important urea pharmacophore at the phenyl ring of **5** and replaces phenyl group (**5**) with pyridine or pyrimidine group (Structure **P**). Based on the chemical design, a 5-pyridin-4-yl-thiazol-2-ylamine series of compounds (**15**) was found to maintain a similar anti-cancer activity to that of **5**. In this study, the structure-activity relationships (SAR) of a series of Structure **P** derivatives are reported. This study has led to the discovery of compound **15a**, which is a multitargeted kinase inhibitor with excellent pharmaceutical properties, good pharmacokinetics (PK) profile, and superior efficacy and tolerability in GIST and AML tumor xenograft models. These promising results demonstrate the potential of **15a** suitable for further preclinical and clinical development.

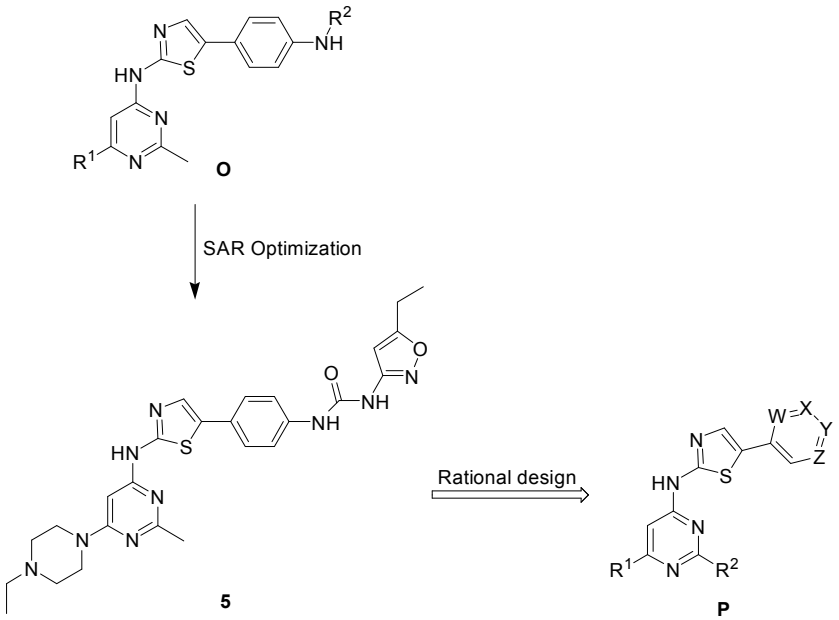

Figure 2. Identification of 5- pyridine-thiazol-2-ylamine derivatives as TKIs.

Chemistry

The general synthetic route to 5-aromatic substituted thiazol-2-ylamine pyrimidines **12-16** (Table 1) is shown in Scheme 1. The synthesis began with the preparation of 5-aromatic substituted thiazol-2-ylamines **9** according to a previously published protocol with some modifications.[42] 2-Aminothiazole **6** was protected with trimethylacetyl chloride using Et_3N to give *N*-thiazol-2-yl-propionamide **7**. The Suzuki coupling of **7** with chloro-substituted pyridine or pyrimidine catalyzed by Pd(0) gave 5-aromatic substituted thiazol-2-ylamides **8**. Amides **8** were hydrolyzed in the presence of a concentrated acid followed by neutralization to yield free 5-aromatic substituted thiazol-2-ylamines **9**. Treatment of 5-aromatic substituted thiazol-2-ylamines **9** or the commercially available **10** with 4,6-dichloropyrimidine or 4,6-dichloro-2-methylpyrimidine in the presence of sodium hydride (NaH) and 1-methyl-2-pyrrolidinone (NMP) at 0 °C yielded 4-monosubstituted pyrimidine derivatives **11**.

The treatment of these derivatives with 2° amines in DMSO at 100 °C or with 2-morpholin-4-yl-ethanol in the presence of KOH and diglyme at 160 °C yielded 4,6-disubstituted pyrimidines **12**−**16**. The synthetic routes to 4-pyridin-3-yl-thiazol-2-ylamine pyrimidine **19** and *N*-(5-pyridin-3-yl-thiazol-2-yl)benzamide **21** (Table 1) are shown in Scheme 1. Displacement of 6-chloro and 4-chloro substituents of 4,6-dichloropyrimidine with sodium salt of 4-pyridin-3-yl-thiazol-2-ylamine **17**[43] and 1-ethylpiperazine, respectively, gave 4,6-disubstituted pyrimidines **19**. Benzoyl chloride **20** with a water-solubilizing 1-methylpiperazine group was employed to acylate amine **9b** in pyridine to yield amide **21**. The freebase forms of compounds **12**−**16**, **19** and **21** were reacted with 6N HCl/CH_3OH aqueous to yield their corresponding hydrochloride salts.

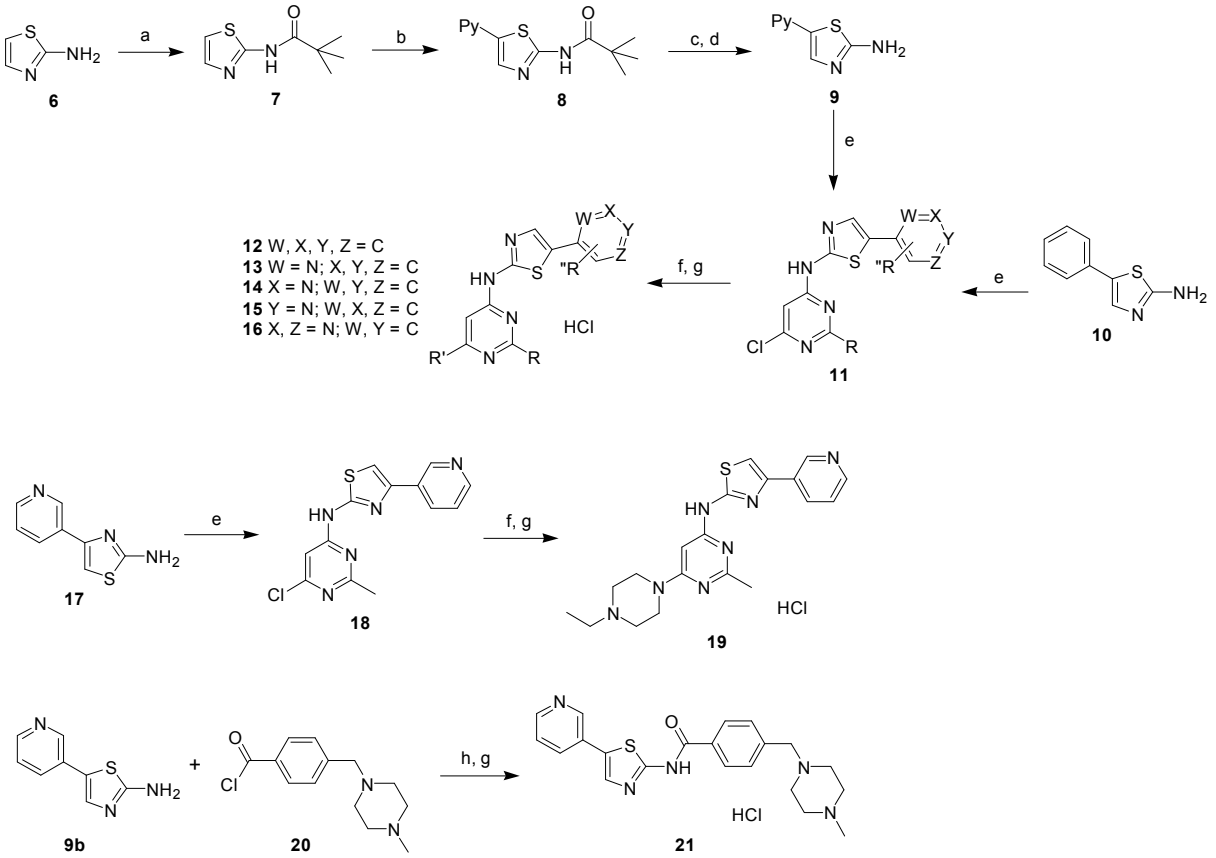

Scheme 1. Reagents and conditions: (a) TEA, CH_2Cl_2, 0 °C to rt; (b)3-Chloropyridine, 4-Chloropyridine or

5-Chloropyrimidine, KOAc, $Pd(PPh_3)_4$, DMAc, 150 °C or 2-Chloropyridine, CsF, $Pd(PPh_3)_4$, DMSO, 160 °C; (c) 12N HCl, H_2O, 110 °C; (d) $NaHCO_3$, H_2O, rt to 50 °C; (e) 4,6-Dichloropyrimidine or 4,6-dichloro-2-methylpyrimidine, NaH, NMP, 0 °C; (f) 2° amines, DMSO, 100 °C or 4-(2-hydroxyethyl)morpholine, KOH, diglyme, 160 °C for **15f**; (g) 6N HCl/CH_3OH, 0 °C; (h) pyridine, 0 °C to rt.

Results and Discussion

***In Vitro* Pharmacology.** As shown in Table 1, the target compounds were tested against c-KIT and FLT3 (in-house kinase assays). In addition, these compounds were further evaluated against the GIST cell line GIST-T1 (expressing a heterozygous deletion in the c-KIT exon 11) and AML cell line MOLM-13 (expressing wild-type FLT3 and FLT3-ITD mutation). The first compound, **12**[44], which lacks a urea pharmacophore of **5**, increased the inhibitory activity against c-KIT (IC_{50} = 24 nM) but significantly lost antiproliferative potency against MOLM-13 cells (GI_{50} = 35 nM) compared to urea **5**. Next, the effects on replacing the phenyl moiety present in **12** with pyridine groups were evaluated. The second position of pyridine attached to the fifth position of thiazole (**13**) exhibited similar inhibitory activities against wild type c-KIT and FLT3 kinases but did result in reduced cellular potencies (GIST-T1 and MOLM-13 GI_{50} = 42 and 36 nM, respectively) relative to **5**. When the nitrogen atom was moved to the third position, **14a** ($R_2 = CH_3$) and **14b** (R_2 = H) were as potent as **5** in the enzymatic assays but were significantly less active in the cellular assays with GI_{50} values of 26−140 nM. Compound **15a** ($R_2 = CH_3$), with the fourth position of pyridine attached to thiazole, exhibited similar inhibitory activities against c-KIT and FLT3 kinases compared to **5** and displayed single digit nanomolar activity against cell lines

GIST-T1 (GI_{50} = 7.1 nM) and MOLM-13 (GI_{50} = 9.4 nM). When compared with **15a**, **15b** (R_2 = H) showed potent inhibitory activities against c-KIT and FLT3 (IC_{50} < 30 nM) but no improvement in cellular potency (GI_{50} > 10 nM).

Next, we examined the effects of water-solubilizing substituents on the fourth position of the pyrimidine ring and compared the potencies of compounds **15c-f** with *N*-ethylpiperazine analog **15a**. *N*-(2-Fluoroethyl)piperazine (**15c**), *N*-(2-hydroxyethyl)piperazine (**15d**), *N*,*N*-dimethylpiperidin-4-amine (**15e**) and 4-(2-hydroxyethyl)morpholine (**15f**) did not affect the inhibitory potencies against c-KIT and FLT3 kinases. Nevertheless, **15e** bearing a *N*,*N*-dimethylpiperidin-4-amine group slightly increased the cellular activities (GIST-T1 GI_{50} = 1.5, MOLM-13 GI_{50} = 3.5 nM), but **15f** bearing morpholine group tethered by a two-carbon ether apparently lost cellular potencies (GIST-T1 GI_{50} = 27, MOLM-13 GI_{50} = 42 nM). In this study, limited water-solubilizing groups were discussed because the effects of some water-solubilizing groups on biological activities, pharmacokinetics and *in vivo* toxicities were fully clarified based on the previous results from the development of 5-phenylthiazol-2-ylamine-based inhibitors (Structure O, Figure 2).[39] Extensive SAR studies were carried out by adding a single methyl substituent on the pyridine ring of **15a** and replacing the pyridine moiety of **15a** with pyrimidine to yield analogs **15g** and **16**, respectively. In comparison with **15a**, 2-methylpyridine **15g** was 2-fold to 4-fold less potent against the c-KIT, FLT3 and MOLM-13 cells but maintained potency against GIST-T1 cells (GI_{50} = 7.7 nM). Pyrimidine **16** exhibited only moderate inhibition of

c-KIT (IC_{50} = 123 nM) and FLT3 (IC_{50} = 163 nM) with a dramatic decrease in cellular potency (GI_{50} > 100 nM).

After optimizing the 5-pyridin-4-yl-thiazol-2-yl series of pyrimidines (compounds **15**, Structure P), we investigated the effects of substitutions on 2-aminothiazole and compared the potencies of compounds **19** and **21** with **14a**, respectively. A significant decrease in both enzymatic activities (IC_{50} > 1,000 nM) and cellular potencies (GI_{50} > 1,000 nM) was observed when the pyridine ring of **14a** was moved from the fifth position to the fourth position (**19**) of the thiazole ring. According to prior reports, the 2-aminothiazole moiety is conformationally well suited to form hydrogen bond interactions with the kinase hinge region of the ATP pocket,[45] and benzamide is a known scaffold for FLT3 kinase inhibitors.[46] Accordingly, we replaced the pyrimidine group with a benzamide group bearing a solubilizing substituent at the *para* position of a benzene ring, yielding benzamide **21**. This approach led to benzamide **21** as only a moderate c-KIT/FLT3 inhibitor with submicromolar activities against GIST-T1 (GI_{50} = 647 nM) and MOLM-13 cells (GI_{50} = 544 nM). Therefore, further modification of lead **21** was not carried out.

As for FDA-approved TKIs for GISTs or AML, compound **1** inhibits tyrosine kinases specifically BCR-ABL, c-KIT and PDGFRα and compounds **2**−**4** are multitargeted TKIs possessing c-KIT/FLT3 dual inhibition (Figure 1). As shown in Table 1, **1** potently inhibited c-KIT and GIST-T1 cells with IC_{50} and GI_{50} values of 53 and 40 nM, respectively. Among these multitargeted TKIs (**2**−**4**), compound **2** exhibited the best enzymatic activities

against c-KIT and FLT3 (IC_{50} < 50 nM) and cellular potencies against GIST-T1 and MOLM-13 cells (GI_{50} < 60 nM). Compounds **3** and **4** showed less potent inhibition toward MOLM-13 (GI_{50} = 887 nM) and GIST-T1 (GI_{50} = 235 nM) cells, respectively. Among the pyridine-substituted 2-aminothiazole analogues listed in Table 1, **15a** and **15c-e** are potent dual inhibitors of c-KIT and FLT3 with less than 10 nM antiproliferative activities in cellular assays. In preliminary studies, the pharmacokinetics, toxicities and/or tumor-inhibiting activities between **15a** and **15c-e** were compared in normal mice or SCID mouse xenografts. The results showed that **15a** caused more significant anti-tumor effects in GIST430 xenografts compared to **15c** and **15d**. Moreover, **15a** exhibited lower toxicity in mice compared to **15c** and **15e,** and the pharmacokinetic profile of **15a** appeared to be more favorable than that of **15d**. Therefore, compound **15a** was selected for further biological activity and *in vivo* efficacy studies.

Table 1. Inhibition of enzymes and cell proliferation with thiazole analogues.

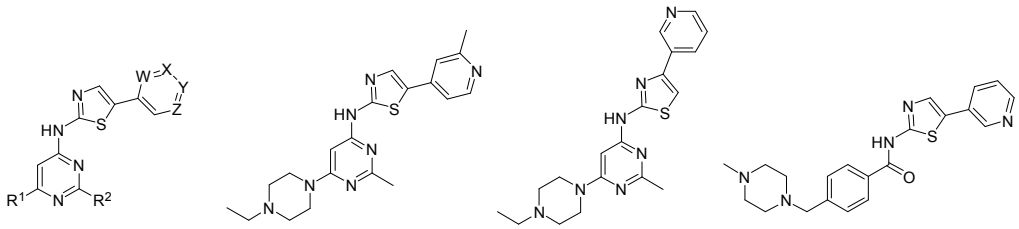

12 W, X, Y, Z = C
13 W = N; X, Y, Z = C
14 X = N; W, Y, Z = C
15 Y = N; W, X, Z = C
16 X, Z = N; W, Y = C

15g **19** **21**

Compd	R^1	R^2	IC_{50} (nM)[a]		GI_{50} (nM)[a]	
			c-KIT	wt-FLT3	GIST-T1	AML MOLM-13
5			97	38	3.2	2.0
12	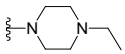	$-CH_3$	24	38	8.0	35

13	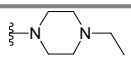	-CH_3	100	24	42	36
14a	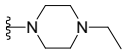	-CH_3	69	63	26	140
14b	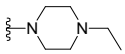	-H	91	60	80	81
15a	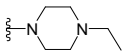	-CH_3	56	30	7.1	9.4
15b	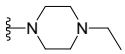	-H	29	20	15	12
15c	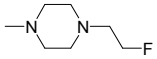	-CH_3	47	37	3.8	7.7
15d	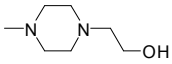	-CH_3	49	43	2.8	6.5
15e	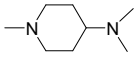	-CH_3	53	35	1.5	3.5
15f	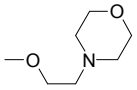	-CH_3	49	35	27	42
15g			100	64	7.7	39
16	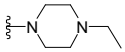	-CH_3	123	163	120	280
19			>1,000	> 1,000	> 1,000	> 1,000
21			107	103	647	544
1 (imatinib)			53	131	40	>1,000
2 (sunitinib)			48	31	38	54
3 (regorafenib)			116	82	119	887
4 (midostaurin)			109	40	235	68

[a]Values are expressed as the mean of three independent determinations and are within ±25%.

Kinase Inhibition Profiles of 15a. To better understand the enzyme inhibition by the potent compound, **15a** was first examined its kinome-wide selectivity profile with DiscoveRx's KinomeScan technology in a panel of 468 kinases and mutants at 100 nM concentration (competition binding assay).[40] The results demonstrated that **15a** was a typical multitargeted tyrosine kinase inhibitor (S score (10) = 0.074 at 0.1 μM, Supporting Information, Figure S1). Because the competition binding assay (KinomeScan) may not fully

reflect inhibitory activity, a continuous kinase enzymatic assay (HotSpot Kinase profiling, Reaction Biology Corporation) was performed to measure **15a**'s inhibition activity against selected 38 protein kinases at a concentration of 100 nM. These 38 kinases covered the major oncogenic kinases of the human protein kinome and showed higher affinity interactions with **15a** (%Ctrl <20, KinomeScan binding assay). The enzyme activity assay results showed that **15a** inhibited 22 kinases by more than 70% at 100 nM out of a panel of 38 tested kinases (Supporting Information, Table S1). Most importantly, the kinase profiling revealed **15a** with potent activity against clinically important wild-type and mutant kinases, including FLT3 (98%), FLT3-D835Y (99%), FLT3-ITD (99%), PDGFRα-T674I (98%), ABL1 (97%), c-Src (94%, IC_{50} = 3 nM), TRKB (93%), TRKA (90%, IC_{50} = 4.9 nM), PDGFRβ (88%), c-KIT (85%), PDGFRα (75%) and PDGFRα-V561D (75%).

Compound 15a Inhibits Enzymatic Activities of a Broad Spectrum of c-KIT Mutants. There are multiple sites of c-KIT mutation in cancers, with some "hot spots" corresponding to the intracellular and extracellular juxtamembrane domains (exons 8, 9 and 11) and the activation loop of the kinase domain (exon 17), which lead to disruption of autoinhibitory mechanisms.[34] The ability of **15a** to potently inhibit activated c-KIT suggested that the inhibitory activity of **15a** among a variety of c-KIT mutants should be examined.[45] Accordingly, various single- or double-mutant isoforms of c-KIT were evaluated for their susceptibility to inhibition by **15a**. As shown in Table 3, compound **15a** more effectively inhibited a broad spectrum of c-KIT mutants bearing single mutations in the JM domain,

ATP-binding pocket and the A-loop. In addition to single c-KIT mutants, **15a** also potently inhibited c-KIT double mutants containing primary V560G and secondary mutations at the A-loop (D816V and N822K), although reduced potency was observed in the V559D/V654A double mutant (54% inhibition at 100 nM concentration, Table 2). Except for ATP binding site mutants and the V559D/V654A double mutant, **15a** was considerably more potent than compound **2** on the inhibition of the other mutants shown in Table 3. Apparently, the inhibition of these mutant forms of c-KIT by compound **3** was not comparable to **15a**, especially toward single mutants V654A, D816H and D816V and double mutants V559D/V654A and V560G/D816V (< 15% inhibition at a concentration of 100 nM).

Table 2. Inhibition of enzymatic activities of c-KIT mutants by **15a**, **2** or **3** (by HotSpot Kinase profiling, Reaction Biology Corporation)

Mutant forms of c-KIT			% inhibition of enzymatic activities					
			15a		**2** (sunitinib)		**3** (regorafenib)	
			100 nM	10 nM	100 nM	10 nM	100 nM	10 nM
JM domain	Exon 11	V560G	93	56	41	8	67	24
ATP binding pocket	Exon 13	V654A	74	49	73	48	14	3
	Exon 13	K642E	94	77	80	60	52	16
	Exon 14	T670I	89	42	93	43	50	9
A-loop	Exon 17	D816H	90	47	56	12	9	0
	Exon 17	D816V	92	49	47	5	10	5
	Exon 17	D820E	98	53	65	16	65	13
	Exon 17	D820Y	99	90	81	36	80	25
	Exon 17	Y823D	99	93	85	28	88	27
	Exon 18	A829P	95	61	43	6	44	4
Double mutant	Exon 11/13	V559D/V654A	54	12	82	32	1	0
	Exon 11/17	V560G/D816V	92	54	52	9	0	0
	Exon 11/17	V560G/N822K	95	61	51	7	50	7

Crystal Structure of c-KIT Kinase in Complex with 15a. The structure of c-KIT kinase in complex with **15a** was obtained, and the statistics for data collection and refinement are summarized in Supporting Information, Table S2. The overall structure of **15a** bound c-KIT adopts an autoinhibited conformation (Figure 3A). The JM region of **15a** is ordered, and the compact hairpin loop conformation resembles that of the autoinhibited c-KIT. The N-terminal half of the hairpin loop (Figure 3A) inserts directly into the interspace between the αC-helix in the N-lobe and the A-loop in the C-lobe. The insertion, together with the other solvent-exposed half (Figure 3A) of the hairpin loop, stabilizes the autoinhibited state by replacing and reorienting the A-loop from an activated to an inactive conformation.

Compound **15a** binds to c-KIT kinase in the ATP-binding site located between the N-lobe and C-lobe (Figure 3B). The thiazolylamine scaffold of **15a** forms two hydrogen bonds with the backbone of Cys673 in the hinge region. In addition, the thiazolylamine group of **15a** also forms hydrophobic interactions with Leu595, Tyr672, Cys673 and Leu799. In particular, the sulfur atom of **15a** forms the sulfur-π interactions with Phe811 in the DFG motif of c-KIT kinase. The pyridine group of **15a** occupies the back pocket of the ATP-binding site by forming a hydrogen bond with the side chain of Lys623. Moreover, **15a** induces a conformational rearrangement of Phe811 to form perpendicular "edge-to-face" aromatic interactions with its pyridine group (Figure 3B). In addition to Phe811, the pyridine group of **15a** also forms hydrophobic interactions with Ala621 and Leu799. The ethylpiperazine group of **15a** is solvent-exposed in the crystal structure of c-KIT, and the

design of this moiety is usually for improvement of the physiochemical properties of compounds. Unlike some type II RTK inhibitors that insert deeply beyond the back pocket of the ATP-binding site,[47] **15a** does not interact with the αC-helix or create any additional hydrophobic pocket that pushes the JM domain away from its autoinhibited conformation. Retaining the JM domain in an autoinhibited conformation may therefore contribute to the high potency of **15a** to inhibit c-KIT kinase activity.

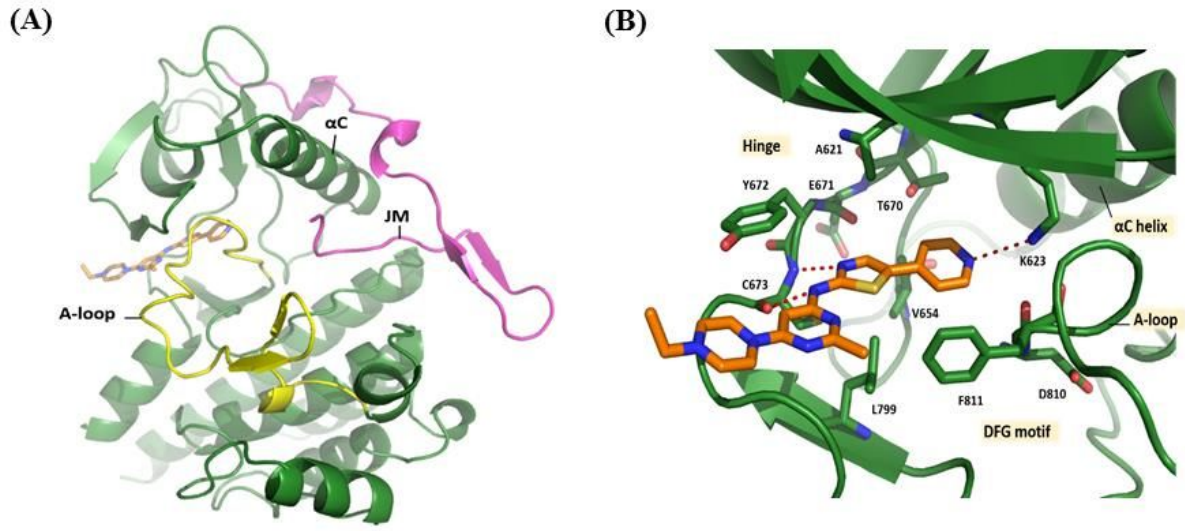

Figure 3. (A) Overall structures of c-KIT in complex with **15a** (PDB code: 6KLA). (B) The interactions of c-KIT with **15a**. The juxtamembrane (JM) domain and activation loop are shown in magenta and yellow, respectively.

Antiproliferative Effects of 15a on c-KIT Mutant GIST Cell Lines. GIST cell lines, including c-KIT mutated GIST882, GIST48, and GIST430, were treated with **15a** and screened for the inhibitory effect of **15a** on cell proliferation via methylene blue assay. Among the three c-KIT-mutated GIST cell lines, GIST882 carries the exon13 K642E mutation. GIST430 has a primary c-KIT exon11 in-frame deletion and a heterozygous secondary exon13 missense mutation (V654A). GIST48 has a primary, homozygous exon 11

missense mutation (V560D) and a heterozygous secondary exon 17 mutation (D820A). The GI_{50} values for GIST cell lines treated with **15a** were 5.0, 17 and 21 nM for GIST882, GIST430, and GIST48, respectively (Table 3). Compared with compounds **1**−**3**, the IC_{50} values of **15a** to suppress the cell proliferation of three c-KIT mutant GIST cell lines are much lower than the three available tyrosine kinase inhibitors used in clinical practice, as shown in Table 3.

Table 3. Inhibitory activity of **1**, **2**, **3** and **15a** against GIST cell lines

cell line	Primary/secondary mutation	GI_{50} (nM)*			
		1 (imatinib)	**2** (sunitinib)	**3** (regorafenib)	**15a**
GIST882	K642E/none	195	64	285	5.0
GIST430	V560-L576del/V654A	929	47	785	17
GIST48	V560D/D820A	625	2,000	> 2,000	21

*Values of GI_{50} are expressed as the mean of three independent experiments and are within ±25%.

As c-KIT is the driving oncogene of c-KIT-mutated GIST cells, we evaluated c-KIT and phosphorylated c-KIT for GIST882, GIST430, and GIST48 cells and found that phosphorylated c-KIT was significantly suppressed by **15a** time-dependently, as shown in Figure 4. GIST cells were treated with 100 nM of **15a** for 24, 48, and 72 h to evaluate the inhibitory effects of **15a** on c-KIT and its downstream signals. Compound **15a** exerted marked suppressive effects on c-KIT phosphorylation in all three GIST cell lines. The downstream signals, the phosphorylation of AKT, and MEK, were suppressed well in GIST882 and GIST430 cells by 100 nM of **15a**. In GIST48 cells, phosphorylated AKT and MEK were suppressed by 100 nM of **15a** at 24 h but recovered at 48 and 72 h. This effect can

be overcome by the use of **15a** at a concentration of 1,000 nM, as shown in Figure 4. Since GIST-T1 cells are sensitive to compounds **1** and **2**, western blot analysis to assess the inhibitory effect of **15a** on phosphorylation of mutant c-KIT is not further tested.

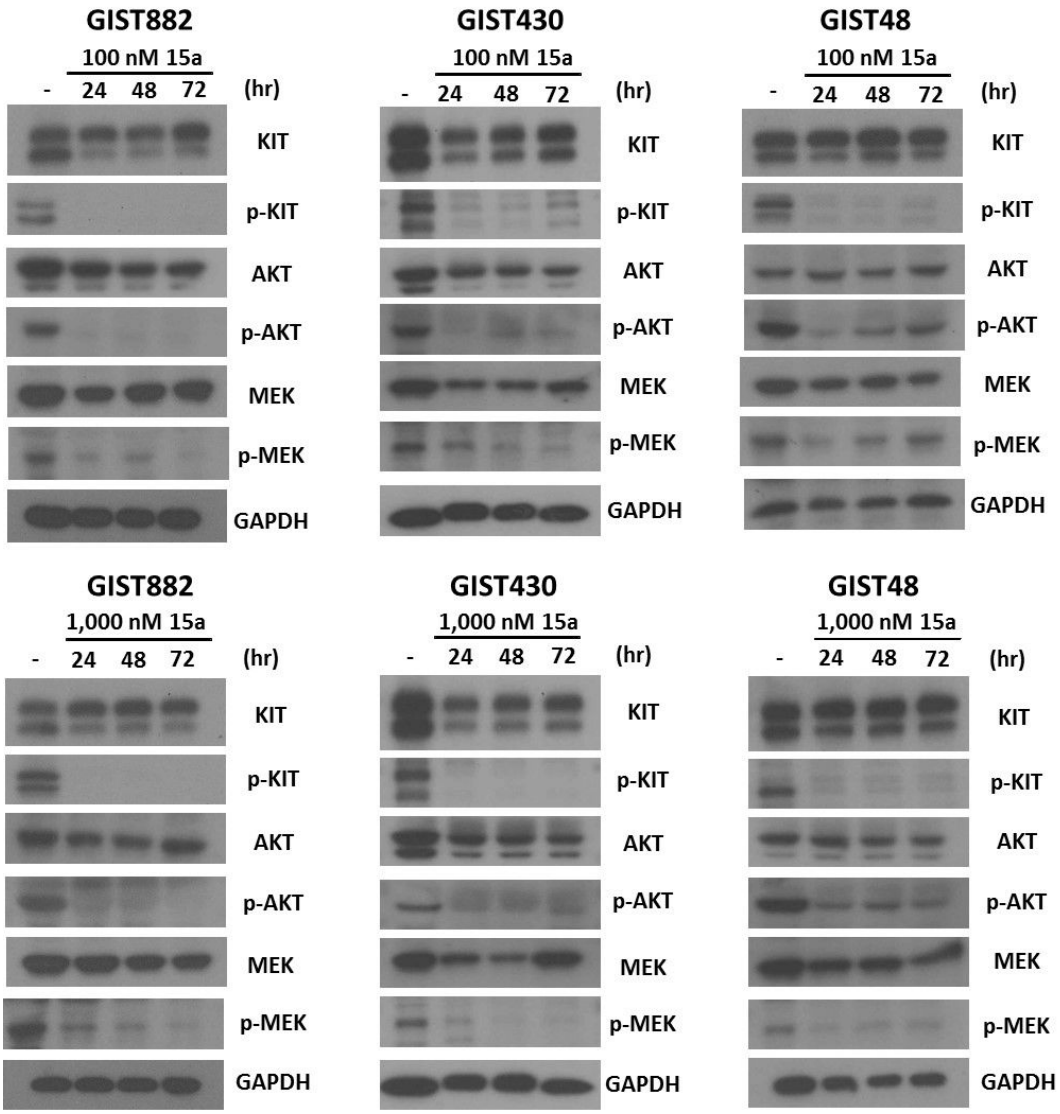

Figure 4. Compound **15a** effectively suppressed c-KIT phosphorylation and its downstream signaling pathways in GIST cell lines.

Antiproliferative Effects of 15a on Leukemia Cell Lines. The antiproliferative activity of **15a** was assessed in a panel of leukemic and transfected BaF3 cell lines (Table 4). Compound **15a** potently inhibited the proliferation of FLT3-ITD-positive AML cell lines

MOLM-13 and MV4;11 with GI_{50} values of 6.4 and 4.9 nM, respectively. In addition, Kasumi-1 cells were sensitive to **15a** with a low GI_{50} value of 12 nM. Kasumi-1 is an AML cell line carrying a c-KIT mutation on codon 822 (N822K). In contrast, **15a** inhibited B-cell acute lymphoblastic leukemia cell line RS4;11 (expressing native FLT3), leukemic monocyte lymphoma cell line U937 (not expressing FLT3) and human chronic myeloid leukemia cell line K562 (expressing wt-BCR/ABL) at significantly higher concentrations (517−2,905 nM), strongly suggesting that **15a** is a dual FLT3/c-KIT inhibitor. The growth inhibitory effects of **15a** on FLT3-driven MOLM-13 and MV4;11 cells were more potent than that of compound **4** (Table 4). Additionally, c-KIT inhibitors **1**−**4** (Figure 1) showed moderate inhibition against Kasumi-1 cells with GI_{50} values of 1,002, 225, 261 and 284 nM, respectively (Table 4).

FLT3-ITD secondary TKD mutants, especially at residues D835 and F691, confer clinical resistance to the FLT3 inhibitors quizartinib and sorafenib.[39] Due to **15a**'s promising potency toward the FLT3-driven AML cell lines, the ability of **15a** to inhibit both D835Y and F691L secondary mutations of FLT3-ITD should be evaluated. In this study, we examined the cellular GI_{50} values of **4** and **15a** against BaF3 cells expressing FLT3-D835Y (activation loop mutation), FLT3-ITD-D835Y (ITD and activation loop mutation) and FLT3-ITD-F691L (ITD and gatekeeper mutation). As shown in Table 4, the cell proliferation–based assays indicated that the sensitivity toward **15a** differed significantly for inhibiting FLT3-D835Y (GI_{50} = 17 nM), FLT3-ITD-D835V (GI_{50} = 92 nM) and FLT3-ITD-F691L (GI_{50} = 152 nM). Compound

15a showed an equal inhibitory effect on the proliferation of BaF3 cells expressing FLT3-D835Y compared to compound **4** (GI_{50} = 16 nM). Nevertheless, the growth inhibitory effects of **15a** on FLT3-ITD-D835Y and -F691L mutants were slightly less potent than **4**, with GI_{50} values of 43 and 47 nM, respectively, as shown in Table 4.

In addition, the antiproliferative activities against other cancer cell lines were also evaluated (Supporting Information, Table S3). The GI_{50} values of **15a** against eleven cancer cell lines ranged from 376 nM (Colo205) to > 20,000 nM (A549 and KYSE-510). Moreover, **15a** had no inhibitory effect on Detroit 551 (normal human skin fibroblast cell), with GI_{50} > 20,000 nM.

Table 4. Potency comparison of **4** and **15a** in cellular assays.

Cell line	GI_{50} (nM)[b]	
Leukemia	**4** (midostaurin)	**15a**
MOLM-13	55	6.3
MV4;11	38	4.9
Kasumi-1[a]	284	12
RS4;11	400	650
U937	1,400	2,905
K562	> 20,000	517
BaF3	GI_{50} (nM)[b]	
Parent/IL3	540	1,100
FLT3-D835Y	16	17
FLT3-ITD-D835Y	43	92
FLT3-ITD-F691L	47	152

[a]Kasumi-1 GI_{50}: **1** = 1,002 nM; **2** = 225 nM; **3** = 261 nM.

[b]Values are expressed as the mean of three independent determinations and are within ±25%.

Because inhibitor of **15** exhibits cytotoxicity in BaF3 cells expressing FLT3 TKD

mutant and FLT3-ITD TKD mutants (Table 4), it was important to verify that the mechanism of cell death was directly linked to the inhibition of FLT3. Next, a western blot analysis was performed using HEK293T cells engineered to express FLT3-WT, FLT3-ITD, FLT3-D835Y or FLT3-ITD-D835Y. As shown in Figure 5, Compound **15a** potently inhibited the phosphorylation of FLT3-WT, FLT3-ITD and FLT3-D835Y with IC_{50} values from 0.1 nM to 1.0 nM. Consistently, **15a** showed moderate potency against autophosphorylation of the FLT3-ITD-D835Y mutant (IC_{50} value of approximately 100 nM), whose inhibition level was closely correlated with antiproliferative effect on BaF3 cells expressing FLT3-ITD-D835Y (GI_{50} = 92 nM, Table 4).

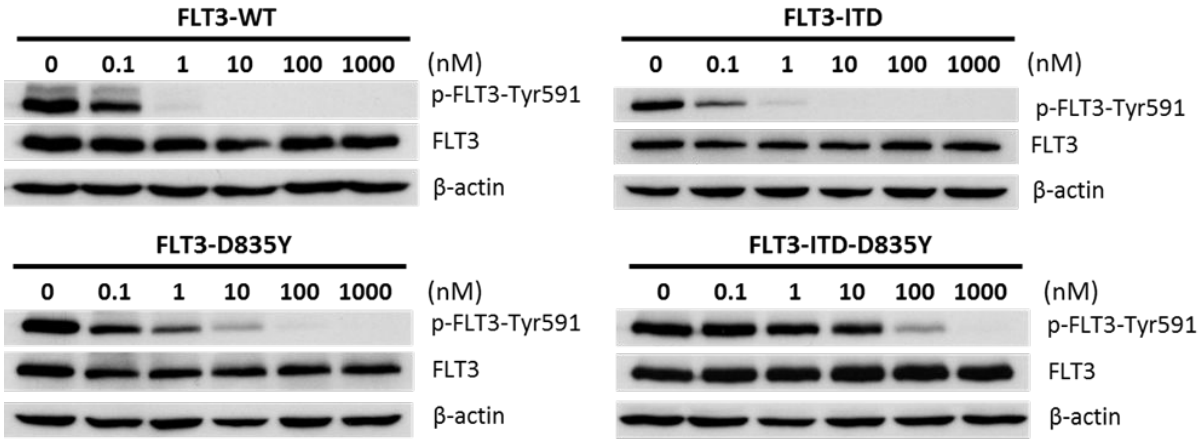

Figure 5. HEK293T cells expressing FLT3-WT, FLT3-ITD, FLT3-D835Y or FLT3-ITD/D835Y were analyzed. FLT3-transfected HEK293T cells were treated with compound **15a** at various concentrations for 1 h. Compound **15a** potently inhibits the FLT3-WT, FLT3-ITD and FLT3-D835Y signaling pathways.

Pharmacokinetics and *In Vivo* Efficacy Studies of 15a. Table 5 shows the pharmacokinetic properties of **15a** evaluated in male Sprague–Dawley rats and ICR mice. In both species, **15a** exhibited high volumes of distribution (V_{ss} = 10.1 L/kg in rats and 14.7

L/kg in mice) and plasma clearances (Cl = 39.6 mL/min/kg in rats and 70.7 mL/min/kg in mice) after intravenous (IV, 2 mg/kg) administration. A single 10 mg/kg oral dose of **15a** was administered as a solution containing 22% hydroxypropyl-β-cyclodextrin in water and absorbed with a moderate half-life in rats ($t_{1/2}$ = 3.9 h) and in mice ($t_{1/2}$ = 4.1 h). The C_{max} (325 ng/mL) and AUC (1955 ng/mL*h) in mice were slightly higher than those in rats, and the oral bioavailability ranged from 36% in rats to 68% in mice. After demonstrating favorable pharmacokinetic properties and excellent cellular potency against GIST and AML cell lines, **15a** was appropriate for continued *in vivo* investigation to determine the antitumor activity of **15a** in a broad panel of GIST and AML xenograft models (Figure 4).

Table 5. Pharmacokinetic profile of compound **15a**.

	IV (dose: 2 mg/kg)				PO (dose: 10 mg/kg)			
Species	$T_{1/2}$ (h)	CL (mL/min/kg)	V_{ss} (L/kg)	$AUC_{(0\text{-inf})}$ (ng/mL*h)	$T_{1/2}$ (h)	C_{max} (ng/mL)	$AUC_{(0\text{-inf})}$ (ng/mL*h)	F (%)
Rats	5.7	39.6	10.1	804	3.9	153	1470	36
Mice	1.6	70.7	14.7	542	4.1	325	1,955	68

First, the *in vivo* pharmacodynamic (PD) effect of **15a** was performed in NOD/SCID mice bearing GIST430 tumors. Three doses of **15a** (10, 20 and 40 mg/kg) were administered orally to subcutaneous GIST430 xenografts and harvested 16 h after **15a** administration. Pharmacodynamic analysis of tumors showed sustained inhibition of p-c-KIT and p-Akt in a dose-dependent response (Figure 6A). These data demonstrated the long-lasting effect of **15a** on c-KIT inhibition *in vivo* and that once-a-day oral dosing was expected to be sufficient for *in vivo* efficacy in the mouse model. To examine its antitumor

efficacy in the GIST430 xenograft model, **15a** was administered orally at a dose of 30 mg/kg once daily (qd) on days 1−2, 5−9 and 12−16. As shown in Figure 6B, rapid tumor regression was observed during the dosing period, with 3 of 5 treated animals exhibiting complete regression (CR) by day 14. There was no tumor regrowth up to day 30, while the 2-treated group (80 mg/kg) began to recur after dosing was halted. In an independent GIST430 xenograft model, treatment of **15a** with a low dose of 15 mg/kg also led to rapid tumor regression, but no CR was found in the low-dose group (Supporting Information, Figure S2). This model was resistant to **1** (approved for GIST first-line treatment) and sensitive to **2** (approved for GIST second-line treatment).[48]

Next, the antitumor efficacy of **15a** was assessed in two GIST patient-derived xenograft (PDX) models. The first PDX model performed in NOD/SCID mice bearing the exon 11 (delW557K558)/exon 17 (Y823D) double mutant was resistant to **1** and **2**. Oral administration of **15a** showed significant antitumor effects at 15 mg/kg and 30 mg/kg qd for 5 days a week for 2 weeks in the PDX model. Treatment with 15 mg/kg dosing caused tumor stasis, whereas tumor regression was observed in the 30 mg/kg dosing group during the second week of treatment followed by slow tumor regrowth starting approximately 7 days after cessation of dosing. At the end of the experiment (day 29), the mean percentage of tumor growth inhibition (TGI) was 76% and 92% in the 15- and 30-mg/kg **15a** administration groups, respectively (Figure 6C). As expected, this PDX model was sensitive to **3** (30 mg/kg),

which is approved for GIST third-line therapy and known to show potency against secondary c-KIT mutants in exon 17 except for D816H/V.[48] The second PDX model was performed in NOD/SCID mice bearing the exon 13 (K642E)/exon 17 (N822K) double mutant. As shown in Figure 6D, **15a** at doses of 15 and 30 mg/kg resulted in tumor stasis by the second week of treatment. Tumors in both groups began to recur after cessation of dosing, with mean values of 80% and 88% TGI being observed in the 15 and 30 mg/kg dosing groups, respectively, on day 29. Apparently, **3** (30 mg/kg) was not sensitive to this PDX model with a 39% TGI on day 29. In the two PDX models, **15a** is well-tolerated at both effective doses.

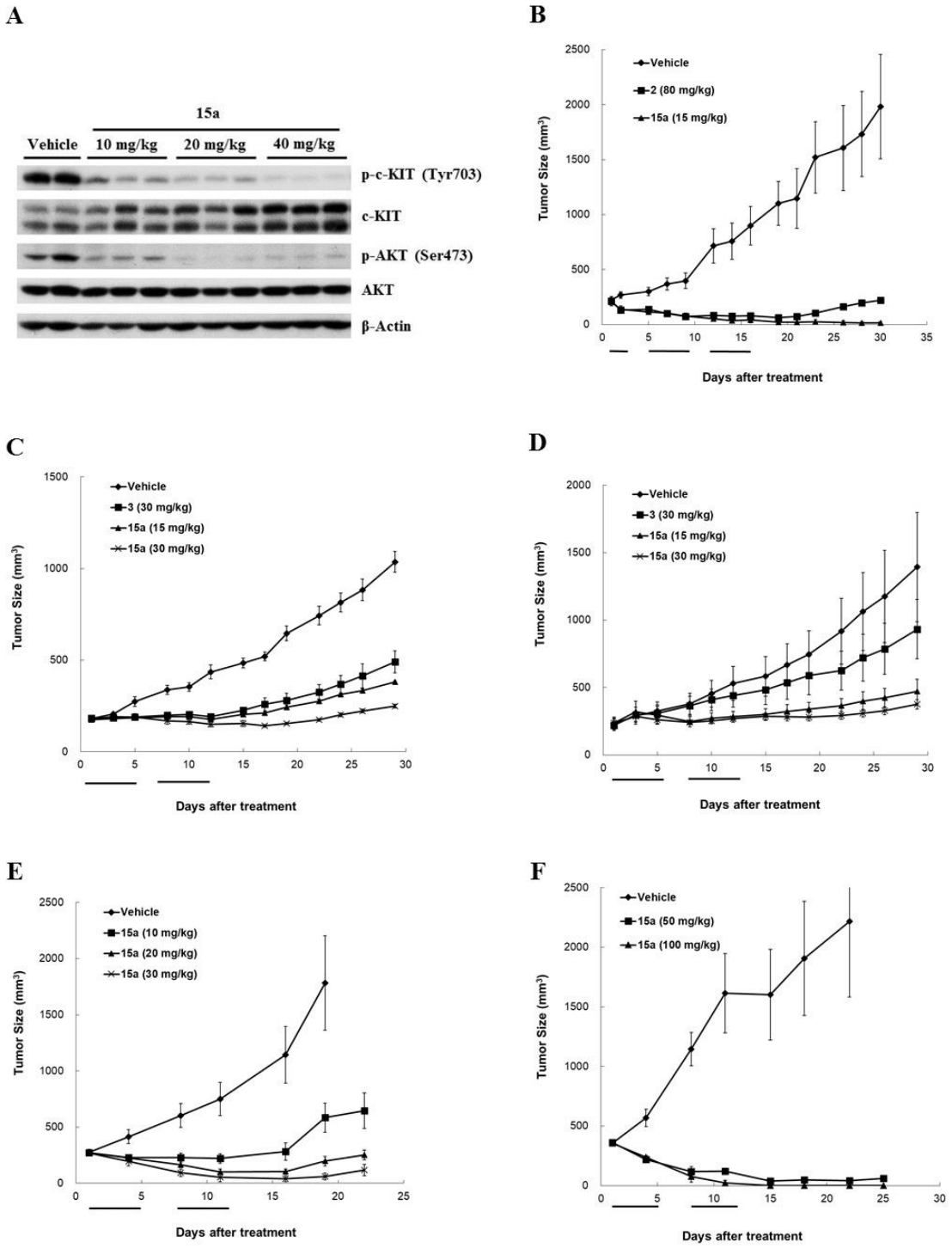

Figure 6. Compound **15a** inhibits the growth of GIST and AML xenografts. (A) A pharmacodynamics study was conducted in the GIST430 xenograft model separately from the efficacy study. Levels of phosphorylated c-KIT (c-KIT-Tyr703) and AKT (AKT-Ser473) were determined by immunoblot. GIST430 xenografts were treated with **15a** (10, 20 and 40 mg/kg) or vehicle for 16 h. Tumors were then harvested, and protein lysates were subjected to immunoblotting for p-c-KIT, total c-KIT, p-AKT, total AKT and β-actin. (B to F) Antitumor activity of **15a** was evaluated against GIST430 xenografts, n = 5/group (B), c-KIT exon 11

(delW557K558)/exon 17 (Y823D) GIST PDX, n = 6/group (C), c-KIT exon 13 (K642E)/exon 17 (N822K) GIST PDX, n = 6/group (D), c-KIT mutated Kasumi-1 AML xenografts, n = 8/group (E), FLT3-ITD mutated MOLM-13 AML xenografts, n = 4/group (F). Mice were treated with **15a** and reference compounds using the dosing levels indicated. The gray bars indicate the dosing schedule for **15a** and reference compounds. The tumor size is expressed as the mean ± SEM.

In AML xenograft models, Kasumi-1 AML xenografts (c-KIT exon 17 N822K) in SCID mice treated with **15a** dosed orally at 10, 20 and 30 mg/kg qd on days 1−5 and 8−12. Treatment with the low dose of 10 mg/kg led to stasis of tumor growth during the administration period, and apparent tumor regression was observed in the 20 and 30 mg/kg dosing groups followed by slow tumor regrowth starting within one week after cessation of dosing (Figure 6E). Four animals in the 30 mg/kg group (n = 8) became and remained tumor-free (CR) through the end of the experiment. In this model, **15a** was well-tolerated at all doses. Finally, a dose-escalation study was conducted to evaluate the *in vivo* efficacy and toxicity of **15a** in nude mice bearing MOLM-13 tumors (FLT3-ITD+). Compound **15a** was administered orally at doses of 50 and 100 mg/kg qd on days 1−5 and 8−12. Treatment started after randomization when tumors had reached an average volume of 370 mm^3. As shown in Figure 6F, apparent tumor regression was observed for the first 5 days in the 50 and 100 mg/kg dosing groups. At 50 mg/kg, near-complete tumor regression was observed in all animals by day 15 (85% tumor regression); no tumor growth resumed after dosing was halted. At 100 mg/kg, complete disappearance of the tumor mass was observed after dosing was halted. Treatment with 100 mg/kg resulted in 4 of 4 treated animals with CR during the 13

days posttreatment observation. No morality and significant loss of body weight (< 10%) was observed in **15a**-treated animals, whereas the maximum tolerated dose of compound **5** (Figure 2) was only 25 mg/kg in nude mouse xenograft models.[39]

Conclusions

A rational design approach successfully identifies a potent, orally bioavailable and multitargeted TKI **15a**, which is expected to exhibit lower toxicity while maintaining significant *in vitro* potency, similar to that of **5**. Importantly, **15a** appears to have superior efficacy and tolerability in GIST and AML tumor xenograft models. In GISTs, preclinical profiling against numerous mutant forms of c-KIT demonstrates that **15a** is active against a broad spectrum of c-KIT mutants, including various secondary mutations that have been identified in **1**-resistant or **2**-resistant GISTs, exhibiting consistent potency to suppress the cell proliferation and c-KIT phosphorylation of GIST882, GIST430 and GIST48 cells. Furthermore, *in vivo* efficacy studies demonstrate that **15a** shows the ability of tumor regression in GIST430 model and exon 11 (delW557K558)/exon 17 (Y823D) PDX model and the ability of suppressing tumor growth in exon 13 (K642E)/exon 17 (N822K) PDX model. In AML, **15a** exhibits potent antiproliferative activities against the c-KIT mutant AML cell line (Kasumi-1) and FLT3-ITD AML cell lines (MOLM-13 and MV4;11). *In vitro* cellular assays and western blot analyses show that **15a** appears to be highly active against clinically relevant FLT3-D835Y but exhibits moderately inhibitory activity against

FLT3-ITD-D835Y and -F691L. Nevertheless, the ability of higher doses of **15a** to induce long-term tumor-free status is observed in the Kasumi-1 and MOLM-13 xenograft models.

Taken together, the excellent *in vitro* and *in vivo* antitumor activities of **15a** suggest that **15a** could be a next-generation drug candidate worthy of clinical evaluation for the treatment of GISTs and AML.

Experimental Section

General Chemistry. All commercial chemicals and solvents are reagent grade and were used without further treatment unless otherwise noted. ^{1}H NMR spectra were obtained with a Varian Mercury-300 or a Varian Mercury-400 spectrometer. Chemical shifts were recorded in parts per million (ppm, δ) and were reported relative to the solvent peak or TMS. LC/MS data were measured on an Agilent MSD-1100 ESI-MS/MS System. High-resolution mass spectra (HRMS) were measured with a Thermo Finnigan (TSQ Quantum) electrospray ionization (ESI) mass spectrometer. Flash column chromatography was done using silica gel (Merck Kieselgel 60, No. 9385, 230-400 mesh ASTM). Reactions were monitored by TLC using Merck 60 F_{254} silica gel glass backed plates (5 × 10 cm); zones were detected visually under ultraviolet irradiation (254 nm) or by spraying with phosphomolybdic acid reagent (Aldrich) followed by heating at 80 °C. All starting materials and amines were commercially available unless otherwise indicated. The purity of compounds was determined by a Hitachi 2000 series HPLC system based on reverse phase C_{18} column (Agilent ZORBAX Eclipse XDB-C18 5 μm,

4.6 mm × 150 mm, condition A) and reverse phase phenyl column (Waters XBridge Phenly 5 μm, 4.6 mm × 150 mm, condition B) under the following gradient elution condition: Mobile phase A-acetonitrile (10% to 90%, 0 to 45 min) and mobile phase B-2 mM NH_4OAc aqueous solution containing 0.1% formic acid (90% to 10%, 0 to 60 min). The flow-rate was 0.5 mL/min and the injection volume was 20 μL. The system operated at 25 °C. Peaks were detected at λ = 254 nm. Purity of all the tested compounds were found to be >95% except for compound **15g** (93.5%, condition B).

2,2-Dimethyl-*N*-thiazol-2-yl-propionamide (7). To a mixture of 2-aminothiazole (**6**, 300 mmol) and triethylamine (330 mmol) in anhydrous CH_2Cl_2 (250 mL) at 0 °C was added trimethylacetyl chloride (310 mmol) and the mixture was stirred at room temperature under an argon atmosphere for 1 h. The mixture was washed with 6 N HCl (60 mL) and the organic layer was separated, dried over $MgSO_4$, and concentrated under reduced pressure. The residue was purified by chromatography on silica gel (20% EtOAc/hexane) to give the desired product **7** as an off-white solid (72%). ^{1}H NMR (300 MHz, DMSO-d_6): δ 11.75 (s, 1H), 7.46 (d, J = 6.0 Hz, 1H), 7.17 (d, J = 6.0 Hz, 1H), 1.22 (s, 9H); MS (ES^+) m/z calcd. for $C_8H_{12}N_2OS$: 184.07; found: 185.1 ($M+H^+$).

2,2-Dimethyl-*N*-(5-pyridin-2-yl-thiazol-2-yl)propionamide (8a). A mixture of 2,2-dimethyl-*N*-thiazol-2-yl-propionamide (**7**, 10 mmol), 2-chloropyridine (10 mmol), cesium fluoride (20 mmol) and tetrakis(triphenylphosphine)palladium(0) (0.5 mmol) in dimethyl sulfoxide (20 mL) was heated at 160 °C under an argon atmosphere for 16 h. The resultant

mixture was partitioned with 0.5N HCl (150 mL) and CH_2Cl_2 (150 mL). The organic layer was separated, dried over $MgSO_4$, concentrated under reduced pressure and purified by chromatography on silica gel (3% acetone /CH_2Cl_2) to give the desired product **8a** as a pale brown solid (20%, precursor of **13**). ^{1}H NMR (300 MHz, DMSO-d_6): δ 11.84 (s, 1H), 8.49 (d, J = 4.5 Hz, 1H), 8.16 (s, 1H), 7.88 (d, J = 7.2 Hz, 1H), 7.82−7.76 (m, 1H), 7.23 (t, J = 6.2 Hz, 1H), 1.24 (s, 9H); MS (ES$^+$) m/z calcd. for $C_{13}H_{15}N_3OS$: 261.09; found: 262.1 (M+H$^+$).

General Procedure for the Preparation of Compounds 8b-d. A mixture of 2,2-dimethyl-*N*-thiazol-2-yl-propionamide (**7**, 30 mmol), 3-chloropyridine, 4-chloropyridine or 5-chloropyrimidine (30 mmol), potassium acetate (120 mmol) and tetrakis(triphenylphosphine)palladium(0) (1.5 mmol) in *N*,*N*-dimethylacetamide (60 mL) was heated at 150 °C under an argon atmosphere for 24 h. Most of solvent was removed by distillation (120 °C /160 mm Hg) and the residue was washed with water (250 mL). The precipitate was collected by filtration, redissolved in 10% CH_3OH/CH_2Cl_2 (200 mL) and filtered through a pad of celite. The filtrate was concentrated under reduced pressure and purified by chromatography on silica gel (1% MeOH/CH_2Cl_2) to give the desired product as an off-white solid (40-85%). Only representative compounds **8b** (precursor of **14**) and **8c** (precursor of **15**) were selected to show their NMR and mass spectra.

2,2-Dimethyl-*N*-(5-pyridin-3-yl-thiazol-2-yl)propionamide (8b). ^{1}H NMR (400 MHz, $CDCl_3$): 9.43 (s, 1H), 8.85 (s, 1H), 8.55 (d, J = 4.8 Hz, 1H), 7.82 (dd, J = 5.6, 4.4 Hz, 1H), 7.70 (d, J = 1.2 Hz, 1H), 7.34 (dd, J = 4.8, 3.2 Hz, 1H), 1.36 (s, 9H); MS (ES$^+$) m/z calcd.

for $C_{13}H_{15}N_3OS$: 261.09; found: 262.2 ($M+H^+$).

2,2-Dimethyl-*N*-(5-pyridin-4-yl-thiazol-2-yl)propionamide (8c). ^{1}H NMR (400 MHz, $CDCl_3$): δ 9.28 (bs, 1H), 8.61 (dd, *J* = 4.8, 1.6 Hz, 2H), 7.84 (s, 1H), 7.42 (dd, *J* = 4.8, 1.6 Hz, 2H), 1.38 (s, 9H); MS (ES^+) m/z calcd. for $C_{13}H_{15}N_3OS$: 261.09; found: 262.1 ($M+H^+$).

General Procedure for the Preparation of Amine Analogues 9. A mixture of **8** (5 mmol) and 12 N HCl (5 mL) in water (5 mL) was heated to reflux for 2 h. Most of solvent was removed under reduced pressure and the residue was diluted with CH_3OH (15 mL). Most of solvent was removed by distillation and the residue was dried in vacuo to give **9** hydrochloride as a pale brown solid. To a stirred suspension of the above solid in water (30 mL) at room temperature was adjusted to pH = 7 with sodium bicarbonate and the mixture was stirred at 50 °C for 2 h. The precipitate was collected by filtration and dried in vacuo to give the desired product as a pale brown solid **9** (85-90%). Only representative compounds **9b** (precursor of **14**) and **9c** (precursor of **15**) were selected to show their NMR and mass spectra.

5-Pyridin-3-yl-thiazol-2-ylamine (9b). ^{1}H NMR (400 MHz, DMSO-d_6): 8.66 (d, *J* = 2.4 Hz, 1H), 8.35 (dd, *J* = 4.8, 1.6 Hz, 1H), 7.81−7.78 (m, 1H), 7.54 (s, 1H), 7.35−7.31 (m, 3H); MS (ES^+) m/z calcd. for $C_8H_7N_3S$: 177.04; found: 178.1 ($M+H^+$).

5-Pyridin-4-yl-thiazol-2-ylamine (9c). ^{1}H NMR (300 MHz, DMSO-d_6): δ 8.41 (dd, *J* = 4.8, 1.5 Hz, 2H), 7.73 (s, 1H), 7.48 (s, 2H), 7.35 (dd, *J* = 4.8, 1.5 Hz, 2H); MS (ES^+) m/z calcd. for $C_8H_7N_3S$: 177.04; found: 178.1 ($M+H^+$).

General Procedure for the Preparation of Pyrimidine Analogues 11 and 18. To

a mixture of **9**, **10** or **17** (4 mmol) and 4,6-dichloropyrimidine (8 mmol) in 1-methyl-2-pyrrolidinone (20 mL) at 0 °C was added sodium hydride (60% in oil, 10 mmol) and the mixture was stirred at 0 °C under an argon atmosphere for 1 h. The reaction was quenched with water (100 mL) at 0 °C and was adjusted to pH = 2 with 6 N HCl. The slurry was adjusted to pH = 7 with sodium bicarbonate and the precipitate was collected by filtration, washed with water (50 mL) and dried in vacuo. The residue was purified by chromatography on silica gel (20% EtOAc/CH_2Cl_2, then 5% to 10% MeOH/CH_2Cl_2 gradient) to give the desired product **11** or **18** as a brown solid (45−60%). Only representative compound **11c** (precursor of **15**) was selected to show its NMR and mass spectrum.

(6-Chloro-2-methylpyrimidin-4-yl)-(5-pyridin-4-yl-thiazol-2-yl)amine (11c). ^{1}H NMR (300 MHz, DMSO-d_6): δ 12.15 (s, 1H), 8.53 (dd, J = 4.5, 1.5 Hz, 2H), 8.18 (s, 1H), 7.59 (dd, J = 4.5, 1.5 Hz, 2H), 6.90 (s, 1H), 2.59 (s, 3H); MS (ES$^+$) m/z calcd. for $C_{13}H_{10}ClN_5S$: 303.03; found: 304.1 (M+H$^+$).

General Procedure for the Preparation of Compounds 12−14, 15a-e, 15g, 16 and 19. A mixture of compound **11** or **18** (2 mmol) and 2° amine (8 mmol) in dimethyl sulfoxide (2 mL) was heated at 100 °C for 1 h. After cooling to room temperature, the mixture was diluted with water (50 mL). The precipitate was collected by filtration, washed with water (10 mL) and dried in vacuo. The residue was purified by chromatography on aluminium oxide (0.5% to 1.5% MeOH/CH_2Cl_2 gradient) to give freebase of each compound **12−14, 15a-e, 15g** or **19** as an off-white solid. To a stirred 6 N HCl (10 mL) at 0 °C was added the

above solid and the solution was filtered through a 0.45 μm PVDF membrane. To the stirred filtrate was added acetone (40 mL) dropwise over the course of 1 h and was stirred for an additional 1 h at 0 °C. The precipitate was collected by filtration, washed with acetone (15 mL) and dried in vacuo to give the HCl salt of each compound **12−14, 15a-e, 15g or 19** as a yellow solid (90−95%).

[6-(4-Ethylpiperazin-1-yl)-2-methyl-pyrimidin-4-yl]-(5-phenyl-thiazol-2-yl)amine hydrochloride (12). Mp 339.1 °C. ^{1}H NMR (400 MHz, DMSO-d_6): δ 11.19 (bs, 1H), 7.74 (s, 1H), 7.56 (d, J = 7.6 Hz, 2H), 7.39−7.35 (m, 2H), 7.25 (d, J = 7.2 Hz, 1H), 6.03 (s, 1H), 3.60−3.40 (m, 4H), 2.40−2.30 (m, 7H), 2.32 (q, J = 6.8 Hz, 2H), 1.00 (t, J = 7.0 Hz, 3H); ^{13}C NMR (100 MHz, DMSO-d_6): δ 165.6, 162.8, 159.2, 157.7, 134.3, 132.7, 130.4, 129.5, 127.3, 125.7, 82.6, 52.4, 52.1, 44.0, 26.1, 12.4; MS (ES$^+$) m/z calcd. for $C_{20}H_{24}N_6S$: 380.18; found: 381.4 (M+H$^+$); HRMS (ESI) calcd. for $C_{20}H_{25}N_6S$: 381.1861; found: 381.1863; HPLC (condition A) t_R = 15.82 min, 100%, (condition B) t_R = 17.50 min, 99.9%.

[6-(4-Ethylpiperazin-1-yl)-2-methyl-pyrimidin-4-yl]-(5-pyridin-2-yl-thiazol-2-yl)amine hydrochloride (13). Mp 295−296 °C. ^{1}H NMR (300 MHz, DMSO-d_6): δ 11.34 (s, 1H), 8.54 (d, J = 4.8 Hz, 1H), 8.32 (s, 1H), 8.01−7.96 (m, 2H), 7.40−7.34 (m, 1H), 6.31 (s, 1H), 4.37 (d, J = 13.2 Hz, 2H), 3.62−3.38 (m, 4H), 3.20−2.90 (m, 4H), 2.47 (s, 3H), 1.26 (t, J = 7.4 Hz, 3H); ^{13}C NMR (75 MHz, D_2O) δ 8.6, 21.8, 42.6, 50.1, 52.3, 84.8, 123.3, 123.5, 124.2, 139.9, 142.1, 144.3, 145.2, 154.4, 157.6, 161.6, 162.7; MS (ES$^+$) m/z calcd. for $C_{19}H_{23}N_7S$: 381.17; found: 382.2 (M+H$^+$); HRMS (ESI) calcd. for $C_{19}H_{24}N_7S$: 382.1814; found: 382.1816

(M+H$^+$); HPLC (condition A) t_R = 15.44 min, 99.3%, (condition B) t_R = 18.35 min, 99.6%.

[6-(4-Ethylpiperazin-1-yl)-2-methylpyrimidin-4-yl]-(5-pyridin-3-yl-thiazol-2-yl) amine hydrochloride (14a). Mp 298−299 °C.^{1}H NMR (400 MHz, DMSO-d_6): δ 11.23 (bs, 1H), 9.15 (s, 1H), 8.68 (d, J = 5.2 Hz, 1H), 8.60 (d, J = 8.0 Hz, 1H), 8.19 (s, 1H), 7.93 (t, J = 6.2 Hz, 1H), 6.21 (s, 1H), 4.35 (d, J = 14.4 Hz, 2H), 3.55 (d, J = 11.6 Hz, 2H), 3.40 (t, J = 13.2 Hz, 2H), 3.13 (t, J = 5.8 Hz, 2H), 3.01 (q, J = 6.9 Hz, 2H), 2.50 (s, 3H), 1.28 (t, J = 6.6 Hz, 3H); ^{13}C NMR (75 MHz, D_2O) δ 9.6, 22.9, 43.5, 51.1, 53.3, 85.2, 125.4, 128.7, 132.1, 137.6, 138.0, 140.2, 142.8, 155.0, 159.2, 162.2, 162.4; MS (ES$^+$) m/z calcd. for $C_{19}H_{23}N_7S$: 381.17; found: 382.2 (M+H$^+$); HRMS (ESI) calcd. for $C_{19}H_{24}N_7S$: 382.1814 ; found: 382.1815 (M+H$^+$); HPLC (condition A) t_R = 12.15 min, 99.8%, (condition B) t_R = 22.47 min, 93.6%.

[6-(4-Ethylpiperazin-1-yl)-pyrimidin-4-yl]-(5-pyridin-3-yl-thiazol-2-yl)amine hydrochloride (14b). Mp 256−257 °C. ^{1}H NMR (300 MHz, DMSO-d_6): δ 11.10 (s, 1H), 8.84-8.81 (m, 2H), 7.63 (s, 1H), 7.49−7.43 (m, 6H), 7.32 (s, 1H), 7.29 (s, 1H), 6.03 (s, 1H), 3.48 (br s, 4H), 2.40−2.30 (m, 9H), 1.01 (t, J = 7.2 Hz, 3H); ^{13}C NMR (75 MHz, DMSO-d_6) δ 12.4, 26.1, 44.0, 52.1, 52.4, 82.6, 110.0, 119.2, 120.2, 125.3, 125.8, 129.1, 130.6, 133.1, 139.0, 139.1, 152.8, 157.7, 158.6, 162.9, 165.6; MS (ES$^+$) m/z calcd. for $C_{27}H_{29}ClN_8OS$: 548.19; found: 549.2 (M+H$^+$); HRMS (ESI) calcd. for $C_{27}H_{30}ClN_8OS$: 549.1952; found: 549.1948 (M+H$^+$); HPLC (condition A) t_R = 25.92 min, 97.4%, (condition B) t_R = 28.18 min, 97.5%.

[6-(4-Ethylpiperazin-1-yl)-2-methyl-pyrimidin-4-yl]-(5-pyridin-4-yl-thiazol-2-yl)a

mine hydrochloride (15a). Mp 343−344 °C. ^{1}H NMR (400 MHz, DMSO-d_6): δ 11.55 (bs, 1H), 8.72 (d, J = 5.6 Hz, 2H), 8.61 (s, 1H), 8.14 (d, J = 5.2 Hz, 2H), 6.27 (s, 1H), 4.35 (d, J = 13.2 Hz, 2H), 3.55 (d, J = 12.0 Hz, 2H), 3.45 (t, J = 13.0 Hz, 2H), 3.13 (t, J = 5.8 Hz, 2H), 3.02 (q, J = 10.0 Hz, 2H), 2.50 (s, 3H), 1.28 (t, J = 6.8 Hz, 3H); ^{13}C NMR (100 MHz, D_2O) δ 8.0, 21.6, 41.8, 49.6, 51.8, 84.1, 120.7, 125.4, 140.2, 141.0, 147.6, 153.8, 158.3, 161.5, 163.2; MS (ES$^+$) m/z calcd. for $C_{19}H_{23}N_7S$: 381.17; found: 382.2 (M+H$^+$); HRMS (ESI) calcd. for $C_{19}H_{24}N_7S$: 382.1814; found: 382.1820 (M+H$^+$); HPLC (condition A) t_R = 9.77 min, 100.0%, (condition B) t_R = 10.61 min, 100.0%.

[6-(4-Ethylpiperazin-1-yl)-pyrimidin-4-yl]-(5-pyridin-4-yl-thiazol-2-yl)amine hydrochloride (15b). Mp 236−241 °C.^{1}H NMR (400 MHz, DMSO-d_6): δ 11.46 (bs, 1H), 8.72 (d, J = 6.8 Hz, 2H), 8.62 (s, 1H), 8.50 (s, 1H), 8.14 (d, J = 6.4 Hz, 2H), 6.41 (s, 1H), 4.33 (d, J = 13.2 Hz, 2H), 3.54 (d, J = 11.6 Hz, 2H), 3.44 (t, J = 13.2 Hz, 2H), 3.20−2.96 (m, 4H), 1.27 (t, J = 7.2 Hz, 3H); ^{13}C NMR (100 MHz, D_2O) δ 8.6, 41.9, 50.2, 52.3, 86.6, 121.5, 126.1, 140.8, 141.9, 148.2, 151.5, 153.0, 159.8, 164.0; MS (ES$^+$) m/z calcd. for $C_{18}H_{21}N_7S$: 367.16; found: 368.1 (M+H$^+$); HRMS (ESI) calcd. for $C_{18}H_{22}N_7S$: 368.1657; found: 368.1661 (M+H$^+$); HPLC (condition A) t_R = 6.70 min, 99.7%, (condition B) t_R = 9.99 min, 99.0%.

{6-[4-(2-Fluoroethyl)-piperazin-1-yl]-2-methyl-pyrimidin-4-yl}-(5-pyridin-4-yl-thiazol-2-yl)amine hydrochloride (15c). Mp 281−283 °C. ^{1}H NMR (300 MHz, DMSO-d_6): δ 11.89 (bs, 1H), 8.73 (d, J = 6.3 Hz, 2H), 8.62 (s, 1H), 8.15 (d, J = 5.7 Hz, 2H), 6.26 (s, 1H), 4.95 (d, J = 47.4 Hz, 2H), 4.38 (s, 2H, overlapping with water peak), 3.70−3.35 (m, 6H), 3.18

(bs, 2H), 2.50 (s, 3H); ^{13}C NMR (100 MHz, D_2O) δ 22.3, 42.1, 51.2, 56.6 (d, *J* = 19 Hz), 77.8 (d, *J* = 166 Hz), 84.6, 121.4, 125.9, 140.8, 141.5, 148.4, 154.3, 159.5, 162.4, 164.0; MS (ES^+) m/z calcd. for $C_{19}H_{22}FN_7S$: 399.16; found: 400.1 ($M+H^+$); HRMS (ESI) calcd. for $C_{19}H_{23}FN_7S$: 400.1720; found: 400.1719 ($M+H^+$); HPLC (condition A) t_R = 8.99 min, 99.7%, (condition B) t_R = 11.44 min, 99.1%.

2-{4-[2-Methyl-6-(5-pyridin-4-yl-thiazol-2-ylamino)pyrimidin-4-yl]-piperazin-1-yl}ethanol hydrochloride (15d). Mp 287−288 °C. ^{1}H NMR (400 MHz, DMSO-d_6): δ 11.03 (s, 1H), 8.73 (d, *J* = 7.2 Hz, 2H), 8.63 (s, 1H), 8.15 (d, *J* = 7.2 Hz, 2H), 6.26 (s, 1H), 4.34 (d, *J* = 12.4 Hz, 2H), 3.82 (t, *J* = 5.2 Hz, 2H), 3.62 (d, *J* = 12.0 Hz, 2H), 3.43 (t, *J* = 12.4 Hz, 2H), 3.30−3.09 (m, 4H), 2.49 (s, 3H); ^{13}C NMR (100 MHz, D_2O) δ 22.2, 42.1, 50.9, 54.8, 58.1, 84.7, 121.3, 126.0, 140.8, 141.6, 148.3, 154.3, 159.0, 162.2, 163.8; MS (ES^+) m/z calcd. for $C_{19}H_{23}N_7OS$: 397.17; found: 398.1 ($M+H^+$); HRMS (ESI) calcd. for $C_{19}H_{24}N_7OS$: 398.1763; found: 398.1767 ($M+H^+$); HPLC (condition A) t_R = 7.92 min, 100.0%, (condition B) t_R = 10.50 min, 100.0%.

[6-(4-Dimethylaminopiperidin-1-yl)-2-methylpyrimidin-4-yl]-(5-pyridin-4-yl-thiazol-2-yl)amine hydrochloride (15e). Mp 323−324 °C. ^{1}H NMR (300 MHz, DMSO-d_6): δ 11.07 (s, 1H), 8.73 (d, *J* = 6.9 Hz, 2H), 8.62 (s, 1H), 8.15 (d, *J* = 6.9 Hz, 2H), 6.25 (s, 1H), 4.43 (d, *J* = 12.9 Hz, 2H), 3.44 (quin, *J* = 5.2 Hz, 1H), 2.94 (t, *J* = 12.5 Hz, 2H), 2.69 (d, *J* = 4.5 Hz, 6H), 2.49 (s, 3H), 2.15 (d, *J* = 10.5 Hz, 2H), 1.60 (q, *J* = 11.0 Hz, 2H); ^{13}C NMR (75 MHz, D_2O) δ 21.7, 25.5, 39.8, 44.4, 62.1, 84.6, 121.2, 126.3, 140.8, 142.0, 148.3, 154.8,

156.3, 161.6, 163.5; MS (ES^+) m/z calcd. for $C_{20}H_{25}N_7S$: 395.19; found: 396.1 ($M+H^+$); HRMS (ESI) calcd. for $C_{20}H_{26}N_7S$: 396.1970; found: 396.1976 ($M+H^+$); HPLC (condition A) t_R = 9.19 min, 98.7%, (condition B) t_R = 11.43 min, 97.6%.

[2-Methyl-6-(2-morpholin-4-yl-ethoxy)pyrimidin-4-yl]-(5-pyridin-4-yl-thiazol-2-yl)amine hydrochloride (15f). To a mixture of **11c** (1 mmol) and 4-(2-hydroxyethyl)morpholine (4 mmol) in diglyme (1 mL) at 100 °C was added potassium hydroxide (10 mmol) and the mixture was stirred at 160 °C under an argon atmosphere for 10 min. The reaction was quenched with water (20 mL) at 0 °C and was adjusted to pH = 2 with 6 N HCl. The slurry was adjusted to pH = 7 with sodium bicarbonate and the precipitate was collected by filtration, washed with water (10 mL) and dried in vacuo. The residue was purified by chromatography on aluminium oxide (0.5% to 1.5% MeOH/CH_2Cl_2 gradient) to give freebase of **15f** as an off-white solid. To a suspension of the solid in MeOH (10 mL) at 0 °C was added 6 N HCl (1 mL) with stirring. Most of solvent was removed under reduced pressure and the residue was treated with EtOH (10 mL). The precipitate was collected by filtration, washed with acetone (10 mL) and dried in vacuo to give the desired product as a yellow solid (48%).

Mp 302−303 °C. ^{1}H NMR (400 MHz, DMSO-d_6): δ 11.61 (s, 1H), 8.74 (d, J = 5.2 Hz, 2H), 8.64 (s, 1H), 8.17 (d, J = 5.2 Hz, 2H), 6.37 (s, 1H), 4.72 (s, 2H), 4.00−3.80 (m, 4H), 3.64−3.42 (m, 4H), 3.16 (bs, 2H), 2.59 (s, 3H); ^{13}C NMR (100 MHz, D_2O) δ 22.6, 52.2, 55.3, 62.7, 63.5, 86.8, 120.8, 126.4, 140.6, 141.3, 148.1, 157.9, 162.6, 164.9, 165.9; MS (ES^+) m/z

calcd. for $C_{19}H_{22}N_6O_2S$: 398.15; found: 399.2 ($M+H^+$); HRMS (ESI) calcd. for $C_{19}H_{23}N_6O_2S$: 399.1603; found: 399.1609 ($M+H^+$); HPLC (condition A) t_R = 8.04 min, 99.9%, (condition B) t_R = 10.52 min, 99.7%.

[6-(4-Ethylpiperazin-1-yl)-2-methyl-pyrimidin-4-yl]-[5-(2-methyl-pyridin-4-yl)thiazol-2-yl]amine hydrochloride (15g). Mp 299−301 °C. ^{1}H NMR (400 MHz, DMSO-d_6): 11.54 (s, 1H), 8.54 (s, 1H), 8.52 (d, J = 3.2 Hz, 1H), 7.99 (s, 1H), 7.95 (d, J = 6.0 Hz, 1H), 6.25 (s, 1H), 4.35 (s, 2H), 3.53 (d, J = 10.8 Hz, 2H), 3.43 (m, 2H), 3.11 (m, 2H), 3.00 (m, 2H), 2.68 (s, 3H), 2.47 (m, 3H), 1.26 (m, 3H); ^{13}C NMR (100 MHz, D_2O) δ 8.8, 18.9, 25.1, 40.9, 49.5, 50.6, 84.2, 109.6, 118.4, 120.9, 125.2, 140.2, 143.7, 147.9, 152.8, 156.7, 161.2, 163.4, 164.9; MS (ES^+) m/z calcd. for $C_{19}H_{23}N_7S$: 395.19; found: 396.2 ($M+H^+$); HRMS (ESI) calcd. for $C_{19}H_{24}N_7S$: 396.1970; found: 396.1975 ($M+H^+$); HPLC (condition A) t_R = 9.35 min, 96.9%, (condition B) t_R = 11.79 min, 93.5%.

[6-(4-Ethylpiperazin-1-yl)-2-methyl-pyrimidin-4-yl]-(5-pyrimidin-5-yl-thiazol-2-yl)amine hydrochloride (16). Mp 354−355 °C. ^{1}H NMR (400 MHz, DMSO-d_6): δ 11.35 (bs, 1H), 9.20−9.03 (m, 3H), 8.09 (s, 1H), 6.28 (s, 1H), 4.40 (s, 2H), 3.56 (d, J = 12.4 Hz, 2H), 3.44 (d, J = 7.4 Hz, 2H), 3.13 (bs, 2H), 3.02 (d, J = 8.0 Hz, 2H), 1.28 (bs, 3H); ^{13}C NMR (100 MHz, D_2O-d_6) δ 8.6, 21.7, 42.3, 50.2, 52.3, 83.9, 123.4, 126.2, 134.8, 152.8, 153.3, 155.1, 158.9, 160.9, 161.3; MS (ES^+) m/z calcd. for $C_{19}H_{23}N_7S$: 382.17; found: 383.3 ($M+H^+$); HRMS (ESI) calcd. for $C_{19}H_{24}N_7S$: 383.1766; found: 383.1764 ($M+H^+$); HPLC (condition A) t_R = 13.07 min, 99.4%, (condition B) t_R = 15.52 min, 98.7%.

[6-(4-Ethylpiperazin-1-yl)-2-methylpyrimidin-4-yl]-(4-pyridin-3-yl-thiazol-2-yl) amine hydrochlorid (19). Mp 72−74 °C. ^{1}H NMR (400 MHz, DMSO-d_6): δ 11.80 (bs, 1H), 11.54 (bs, 1H), 9.28 (s, 1H), 8.94 (d, J = 8.4 Hz, 1H), 8.84 (d, J = 5.2 Hz, 1H), 8.15−8.07 (m, 2H), 6.31 (bs, 2H), 4.35 (d, J = 14.0 Hz, 2H), 3.55 (d, J = 12.0 Hz, 2H), 3.45 (t, J = 13.0 Hz, 2H), 3.15−3.07 (m, 2H), 3.00 (q, J = 10.0 Hz, 2H), 2.49 (s, 3H), 1.27 (t, J = 7.4 Hz, 3H); ^{13}C NMR (100 MHz, D_2O) δ 8.7, 22.0, 42.5, 50.1, 52.3, 83.4, 114.4, 127.6, 132.4, 137.8, 139.7, 142.1, 142.3, 153.1, 158.1, 160.2, 160.6; MS (ES$^+$) m/z calcd. for $C_{19}H_{23}N_7S$: 381.17; found: 382.1 (M+H$^+$); HRMS (ESI) calcd. for $C_{19}H_{24}N_7S$: 382.1814; found: 382.1798 (M+H$^+$); HPLC (condition A) t_R = 12.76 min, 98.3%, (condition B) t_R = 13.95 min, 98.4%.

4-(4-Methylpiperazin-1-ylmethyl)-N-(5-pyridin-3-yl-thiazol-2-yl)benzamide hydrochloride (21). To a solution of **9b** (2 mmol) in pyridine (5 mL) at 0 °C was added 4-(4-methyl-piperazin-1-ylmethyl)benzoyl chloride (**20**, 3 mmol) and the mixture was stirred at room temperature under an argon atmosphere for 1 h. Most of solvent was removed under reduced pressure and the residue was washed with 1 N $NaHCO_3$ (10 mL). The precipitate was collected by filtration and purified by chromatography on silica gel (5% to 10% MeOH/CH_2Cl_2 gradient) to give freebase of **21** an off-white solid. To a suspension of the solid in MeOH (20 mL) at 0 °C was added 6 N HCl (2 mL) with stirring. Most of solvent was removed under reduced pressure and the residue was treated with EtOH (15 mL). The precipitate was collected by filtration, washed with acetone (15 mL) and dried in vacuo to give the desired product as a yellow solid (75%).

Mp 266−267 °C. ^{1}H NMR (400 MHz, DMSO-d_6): δ 12.02 (bs, 1H), 9.20 (s, 1H), 8.73 (d, J = 5.2 Hz, 1H), 8.65 (d, J = 8.4 Hz, 1H), 8.36 (s, 1H), 8.20 (d, J = 8.4 Hz, 2H), 7.94 (q, J = 4.5 Hz, 1H), 7.88 (d, J = 8.0 Hz, 2H), 4.50 (bs, 2H), 3.70−3.35 (m, 8H), 2.81 (bs, 3H); MS (ES$^+$) m/z calcd. for $C_{21}H_{23}N_5OS$: 393.16; found: 394.1 (M+H$^+$); HRMS (ESI) calcd. for $C_{21}H_{24}N_5OS$: 394.1702; found: 394.1701 (M+H$^+$); HPLC (condition A) t_R = 11.78 min, 98.3%, (condition B) t_R = 14.96 min, 99.7%.

Biochemical Kinase Assays. The recombinant His-c-KIT (residues T544−end) was expressed in Sf9 insect cell. The kinase assay was carried out in 96-well plates at 30 °C for 150 min in a final volume of 10 μL including the following components: 250 ng c-KIT proteins, 40 mM Tris−HCl, pH 7.4, 2 mM $MnCl_2$, 2 mM DTT, 20 mM $MgCl_2$, 0.1 mg/mL bovine serum albumin, 40 μM poly(Glu,Tyr) 4:1, 1 mM Na_3VO_4, and 20 μM ATP. Following incubation, 5 μL ADP-Glo Reagent (Promega) was added and the mixture was incubated at 25 °C for 40 min. 10 μL KDR Reagent was added and the mixture was incubated 25 °C for 30 mins. Add 15 μL buffer and mixture. A 30-μL aliquot of each reaction mixture was transferred to a black microtiter plate and the luminescence was measured on Wallac Vector 1420 multilabel counter. The recombinant GST-FLT3 (residues Y567−S993) containing kinase domain was expressed in Sf9 insect cells transfected the baculovirus containing pBac-PAK8-GST-FLT3-KD plasmid. The FLT3 WT Kinase-Glo assays were carried out in 96-well plates at 30 °C for 4 h and tested compound in a final volume of 50 μL including the following components: 75 ng GST-FLT3 proteins, 25 mM HEPES, pH 7.4, 4 mM $MnCl_2$, 10 mM $MgCl_2$, 2 mM DTT, 0.02% Triton X-100, 0.1 mg/mL bovine serum albumin, 25 μM Her2 peptide substrate, 0.5 mM Na_3VO_4, and 1 μM ATP. Following incubation, 50 μL Kinase-Glo Plus Reagent (Promega, Madison, WI, USA) was added and the mixture was

incubated at 25 °C for 20 min. A 70-μL aliquot of each reaction mixture was transferred to a black microtiter plate and the luminescence was measured on Wallac Vector 1420 multilabel counter (PerkinElmer, Shelton, CT, USA).

Hotspot Kinase Profiling Assays. In vitro kinase profiling of c-KIT mutants and 38 kinases was performed at Reaction Biology Corporation. The assay conditions and protocol are given in the supporting information.

Kinase Expression, Purification and Crystallization. c-KIT kinase domain (residues 547−935), with the kinase insertion domain (residues 694−753) being deleted and replaced by a 6-nucleotide fragment encoding Thr-Ser, was cloned into pBacPAK8 vector to generate recombinant baculovirus for protein expression.. A 6x-histidine tag followed by a thrombin cleavage site was also added in-frame to the N-terminal of cloned c-KIT. Recombinant c-KIT was expressed in Sf9 insect cells and the cell pellets were suspended in Tris buffer (25 mM Tris-HCl, pH7.6, 250 mM NaCl, and 0.5 mM TCEP) and lysed by sonication. The supernatant was loaded onto HisTrap HP column (GE Life Sciences) and c-KIT containing His tag was eluted by a liner imidazole gradient. Thebuffer was then exchanged to thrombin cleavage buffer (20 mM Tris-HCl, pH 8.4, 150 mM NaCl, and 2.5 mM $CaCl_2$) and cleaved by thrombin at 4 °C for overnight. After removal of the His tag, buffer of recombinant c-KIT proteins was exchanged to 25 mM Tris-HCl, pH7.6, 250 mM NaCl, and 5 mM DTT.

Recombinant c-KIT kinase was co-crystallized with **15a** by a hanging drop method. 7.0 mg/mL of c-KIT proteins were pre-incubated with 0.7 mM **15a** on ice and mixed with equal volume of reservoir solution (20% PEG3350 and 100 mM sodium citrate tribasic dihydrate, pH 5.6) plus 2% benzamidine hydrochloride as an additive. Crystals were grown at 18 °C and immersed quickly in the reservoir solutions with additional cryoprotectants containing 8% ethylene glycol before being flash-frozen in liquid nitrogen. The X-ray diffraction data sets were collected at beamline TPS05A (NSRRC, Taiwan) and processed

with the HKL2000 program. The initial phases of c-KIT kinase domain structures were obtained by molecular replacement using the PHENIX package. The previously reported c-KIT structure (PDB code 1T46) was used as a template. Structure refinement was performed using PHENIX and model building was carried out by COOT).

Cell Lines and Cell Culture. GIST882, GIST430 and GIST48 cells were gifts from Dr. Jonathan A. Fletcher (Harvard Medical School, US). They were all cultured in incubators maintained at 37 °C and 5% CO_2. GIST882 cells were cultured in RPMI-1640 supplemented with 20% fetal bovine serum (FBS). GIST48 cells were cultured with F10 supplemented with 20% FBS, 0.5% Mito, serum extender (BD Bioscience, 355006) and 1% pituitary extract bovine (BD Bioscience 354123). GIST430 cells were cultured in IMDM supplemented with 20% FBS.

MV4;11, Kasumi-1, RS4;11, U937, K562, BaF3 and HEK293T cell lines were obtained from American Type Culture Collection (ATCC, Manassas, VA, USA). MOLM-13 cell line was purchased from the Deutsche Sammlung von Microorganismen und Zellkulturen GmbH (DSMZ, Braunschweig, Germany). The GIST-T1 cell line was obtained from COSMO BIO CO., LTD (Tokyo, Japan). The GIST-T1, MOLM-13, MV4:11, RSV4;11, U937, K562, BaF3, BaF3/FLT3-ITD-F691L and BaF3/FLT3-ITD-D835Y cells were maintained in RPMI 1640 medium supplemented with 10% fetal bovine serum (FBS), 10 U/mL penicillin, and 100 μg/mL streptomycin at 37 °C and 5% CO_2. The kasumin-1 cells were cultured in RPMI 1640 medium supplemented with 20% fetal bovine serum (FBS), 1 mM Hepes, 1 mM sodium pyruvate, 10 U/ml penicillin, and 100 μg/ml streptomycin. The HEK293T and

FLT3-transfected HEK293T cells were cultured in DMEM (Invitrogen, USA) medium with 10% FBS fetal bovine serum.

MTS Cell Viability Assay. GIST882, GIST430 or GIST48 cells (4×10^4) were treated with different dosage of **15a**, imatinib, sunitinib or regorafenib. The treated GIST882 cells were incubated for 144 h and GIST48 and GIST430 cells were incubated for 120 h at 37 °C in 5% CO_2. Cell proliferation was determined by incubating the cells with methylene blue (Clontech, CA, US) for 1 h. The absorbance was measured at 450 nm using SpectraMax M5 microplate reader (Molecular Devices, US).

Cell viability assay was performed by seeding 1×10^4 cells (MOLM-13, MV4:11, Kasumi-1, RS4;11, U937, K562, BaF3, BaF3/FLT3-D835Y, BaF3/FLT3-ITD-D835Y and BaF3/FLT3-ITD-F691L) per well in a 96-well culture plate. GIST-T1 cells were seeded in 96-well culture plate at density of 8×10^3 cells/100 μL. After 16 h, cells were then treated with vehicle or various concentrations of compound in medium for 72 h. The viable cells were quantitated using the CellTiter 96 AQueous MTS method (Promega, Madison, WI, USA) according to the manufacturer's recommended protocol. The results were determined by measuring the absorbance at 490 nm using a plate reader (Victor2; PerkinElmer, Shelton, CT, USA). The IC_{50} value was defined as the amount of compound that caused 50% reduction in cell viability in comparison with DMSO-treated (vehicle) control and was calculated using Prism version 6 software (GraphPad, San Diego, CA, USA).

Western Blot Analysis. GIST882, GIST430 or GIST48 cells were treated with 1 μM or 100 nM of **15a** at the pre-specified time points to evaluate the time effect. Cell lysates were extracted with the CelLytic^{TM} M mammalian cell lysis/extraction solution purchased from Sigma (St. Louis, MO, USA). The cell lysates were resolved in SDS-PAGE gel and transferred to PVDF membranes (Bio-Rad, CA, US). Non-specific binding was blocked using 5% BSA/PBST for 1 hour, washed four times with 0.1% Tween-20/PBS, and followed by incubating with designed primary antibodies overnight at 4 °C. The immunocomplexes were detected by probing with anti-mouse or -rabbit IgG conjugated with horseradish peroxidase, and visualized using the Enhanced Chemiluminescence detection kit (PerkinElmer Western Lightning Plus-ECL; MA, US). The primary antibodies, p-Akt, p-MEK, and p-MAPK were purchased from Cell signaling (Danvers, US). Antibodies against GAPDH was purchased from Santa Cruz (Texas, US). Antibody against p-c-KIT was purchased from Invitrogen (Frederick, US). c-KIT was purchased from DAKO (Carpinteria, US).

Transfected HEK293T cells were lysed in lysis buffer (50 mM Tris, pH 8.0, 150 mM NaCl, 1% Triton X-100, 0.5% sodium deoxycholate, 0.1% SDS, 1 mM sodium orthovanadate, 1 mM PMSF, and 1 mM DTT). Protein lysates were resolved by SDS-PAGE and transferred onto a polyvinylidene difluoride (PVDF) membrane (Millipore, Bedford, MA, USA). The membranes were immunoblotted with appropriate antibodies and detected using the SuperSignal reagent (Pierce, Rockford, IL, USA) followed by exposure to X-ray film. The anti-pFLT3-Tyr591 (#3461, Cell Signaling Technology) antibody was purchased for Western

blotting analysis.

Pharmacokinetics. Male ICR mice (25−35 g) and male Sprague–Dawley rats (300−400 g) were obtained from BioLASCO (Taiwan Co., Ltd, Ilan, Taiwan). The animal studies were performed according to NHRI institutional animal care and committee-approved procedures. Rats were surgically prepared with a jugular-vein cannula one day before dosing. Rats and mice were fasted overnight (for approximately 18−20 h) before dosing. Water was available *ad libitum* throughout the experiment. Food was provided at 4 h after dosing. A single 2.0 mg/kg and 10 mg/kg dose of compound, as a PEG400/DMA (80/20, v/v) solution, was separately administered to rats and mice. The groups of 3 rats each routes and a total of 33 and 27 mice for intravenously (IV) and oral gavage (PO), respectively. Each rat received 2 or 10 mL of the dosing solution per kg of body weight and each mouse was given 100 μL and 200 μL of dosing solution by intravenous injection and by gavage, respectively. At 0 (before dosing), 2, 5 (IV only), 15, and 30 min and at 1, 2, 4, 6, 8, 16 (mice only) and 24 h after dosing, a blood sample (0.15 mL) was collected from each rat through the jugular-vein cannula and ~500 μL was collected from groups of 3 mice at each time point by cardiac puncture and stored in ice (0−4 °C). Immediately after collecting the blood sample, 150 mL of physiological saline (containing 30 Units of heparin per ml) was injected into the rat through the jugular-vein cannula. Plasma was separated from the blood by centrifugation (14 000 g for 15 min at 4 °C in a Beckman Model AllegraTM 6R centrifuge) and stored in a freezer (-20 °C). All samples were analyzed for the parent drug by LC-MS/MS. Data were acquired

through selected reaction ion monitoring. Plasma concentration data were analyzed with non-compartmental method.

Pharmacodynamic Studies. PD Studies were performed separately from the efficacy studies. GIST430–bearing NOD/SCID male mice were prepared by the same method as the efficacy study. Animals were randomized when average tumor volume reached > 100 mm^3, followed by oral dosing of **15a** or vehicle. Tumors were collected at 16 h after administration. Tumors were excised, weighed and stored at -80 °C. A portion of the tumor tissue was rinsed with phosphate-buffered saline buffer and then homogenized in RIPA buffer (#9806, Cell Signaling Technology) with protease/phosphatase inhibitors (B14001/B15001, Biotool, Houston, TX, USA). After the protein concentrations was quantified by Pierce™ BCA (bicinchoninic acid) assay kit (#23227, Thermo Scientific, Rockfold, IL, USA), 30 μg protein lysate was subject to SDS–polyacrylamide gel electrophoresis, followed by immunoblotting with antibodies (anti-c-KIT (#3308, Cell Signaling Technology), anti-p-c-KIT-Tyr703 (#3073, Cell Signaling Technology), and anti-β-actin (MA5-15739, Thermo Fisher) and then detected using the SuperSignal reagent (Pierce, Rockford, IL, USA) followed by exposure to X-ray film and quantify the changes of c-KIT phosphorylation.

Animal Studies. The animal use protocol was approved by National Health Research Institutes (Protocol No: NHRI-IACUC-106076-A). NOD/SCID male mice were obtained from the National Laboratory Animal Center, Tainan, Taiwan. NOD/SCID female mice were purchased from Jackson Laboratories, Bar Habor, ME, USA. SCID male mice and

athymic nude male mice were purchased from BioLASCO, Ilan, Taiwan. Compound **15a**, sunitinib (Selleckchem) and regorafenib (Ark Pharm, Inc.) were formulated in 20% (2-hydroxypropyl)-β-cyclodextrin (Sigma). For GIST430 xenograft model, GIST430 cells (2 × 10^7/mouse) were injected subcutaneously into NOD/SCID (6 to 8 weeks old) male mice. For the GIST exon 11/17 (GS5108 model) and exon 13/17 (GS5107 model) PDX studies, GS5108 cells (1 × 10^5/mouse) and GS5107 cells (9.1 × 10^4/mouse) were injected subcutaneously into NOD/SCID (6 to 8 weeks old) female mice. Both the PDX models were performed at Crown Biosciences. For the mouse xenograft model using leukemia cell lines, Kasumi-1 and MOLM-13 cells (1 × 10^6/mouse) were injected subcutaneously into SCID and athymic nude (6 to 8 weeks old) male mice, respectively. Animals were randomized when average tumor volume reached approximately 210 mm^3 (n = 5) for GIST430 tumors, approximately 180 mm^3 (n = 6) for GS5108 tumors, approximately 230 mm^3 (n = 6) for GS5107 tumors, approximately 250 mm^3 (n = 8) for Kasumi-1 tumors, approximately 370 mm^3 (n = 4) for MOLM-13 tumors, followed by oral dosing of compounds at the indicated dose levels and schedules shown in Figure 6.

Tumor size was measured with a digital caliper, and the tumor volume in mm^3 was calculated by the formula: Volume = (length x width^2)/2. All mice were monitored daily for signs of toxicity. Body weight and tumor size were measured twice or three times a week. Daily observations of health changes are possible during experimental time. At the end of the studies, animals will then be euthanized by carbon dioxide inhalation followed by cervical

dislocation.

Associated Content

Supporting Information

Material and methods of Hotspot kinase profiling assays and antiproliferation assays, Figure S1 listing the TREEspot interaction maps and selectivity score of **15a**, Table S1 listing kinase inhibition profile of compound **15a**, Table S2 listing statistics of X-ray diffraction data and structure refinement for c-KIT complex, Table S3 listing cell viability of cancer cell lines and normal cell line treated with **15a**, Figure S2 compared the antitumor effect of **15a** (15 mg/kg) and **2** (40 mg/kg) on GIST430 xenograft mouse model, ^{1}H and ^{13}C NMR spectrum of **15a** and HPLC reports for the purity check of compounds **15a**−**g**.

Accession Codes

6KLA (c-KIT/**15a)**.

Authors will release the atomic coordinates and experimental data upon article publication.

Corresponding Authors

For W. T. Jiaang: phone, +886-37-246-166 ext 35712; fax, +886-37-586-456; E-mail, wtjiaang@nhri.org.tw

For H. J. Tsai: phone, +886-6-208-3422 ext 65149; fax, +886-6-208-3427; E-mail: hjtsai@nhri.org.tw

Acknowledgments

We thank the staff of beamlines TPS05A, BL15A1 and BL13B1 at the National Synchrotron Radiation Research Center (NSRRC), Taiwan, and SP44XU at the Spring-8, Japan, for technical assistance. The National Health Research Institutes, Ministry of Economic Affairs and National Science Council of Taiwan (MOST 103-2325-B-400 -013 -) financially supported the study.

Abbreviations Used

GIST, gastrointestinal stromal tumor; AML, acute myeloid leukemia; c-KIT, stem cell factor receptor; FLT3, fms-like tyrosine kinase-3; TKI, tyrosine kinase inhibitor; PFS, progression free survival; OS, overall survival; PDGFR, platelet-derived growth factor receptor; mOS, median overall survival; CSF1R (FMS), colony stimulating factor receptor; RTK, receptor tyrosine kinase; ITDs, internal tandem duplications; AL, activation loop; TKD, tyrosine kinase domain; CBF, core binding factor; SAR, structure-activity relationships; PK, pharmacokinetics; PD, pharmacodynamics; qd, once daily; CR, complete regression.

References

(1) Joensuu, H.; Hohenberger, P.; Corless, C. Gastrointestinal stromal tumour. *Lancet* **2013**, *382*, 973−983.

(2) Miettinen, M.; Lasota, J. Gastrointestinal stromal tumors – definition, clinical, histological, immunohistochemical, and molecular genetic features and differential diagnosis. *Virchows Arch.* **2001**, *438*, 1−12.

(3) Hirota, S.; Isozaki, K.; Moriyama, Y.; Hashimoto, K, Nishida, T.; Ishiguro, S.; Kawano, K.; Hanada, M.; Kurata, A.; Takeda, M.; Muhammad Tunio, G.; Matsuzawa, Y.; Kanakura, Y.; Shinomura, Y.; Kitamura, Y. Gain-of-function mutations of c-kit in human gastrointestinal stromal tumors. *Science* **1998**, *279*, 577−580.

(4) Joensuu, H.; Roberts, P. J.; Sarlomo-Rikala, M.; Andersson, L. C.; Tervahartiala, P.; Tuveson, D.; Silberman, S.; Capdeville, R.; Dimitrijevic, S.; Druker, B.; Demetri, G. D. Effect of the tyrosine kinase inhibitor STI571 in a patient with a metastatic gastrointestinal stromal tumor. *N. Engl. J. Med.* **2001**, *344*, 1052−1056.

(5) Poveda, A.; García Del Muro, X.; López-Guerrero, J. A.; Cubedo, R.; Martínez, V.; Romero, I.; Serrano, C.; Valverde, C.; Martín-Broto, J. GEIS guidelines for gastrointestinal sarcomas (GIST). *Cancer Treat. Rev.* **2017**, *55*, 107-119.

(6) Demetri, G. D.; von Mehren, M.; Blanke, C. D.; Van den Abbeel,e A. D.; Eisenberg, B.; Roberts, P. J.; Heinrich, M. C.; Tuveson, D. A.; Singer, S.; Janicek, M.; Fletcher, J. A.; Silverman, S. G.; Silberman, S. L; Capdeville, R.; Kiese, B.; Peng, B.; Dimitrijevic, S.; Druker, B. J.; Corless, C.; Fletcher, C. D.; Joensuu, H. Efficacy and safety of imatinib mesylate in advanced gastrointestinal stromal tumors. *N. Engl. J. Med.* **2002**, *347*, 472−480.

(7) Blanke, C. D.; Demetri, G. D.; von Mehren, M.; Heinrich, M. C.; Eisenberg, B.; Fletcher, J. A.; Corless, C. L.; Fletcher, C. D.; Roberts, P. J.; Heinz, D.; Wehre, E.; Nikolova, Z.; Joensuu, H. Long-term results from a randomized phase II trial of standard-versus higher-dose imatinib mesylate for patients with unresectable or metastatic gastrointestinal stromal tumors expressing KIT. *J. Clin. Oncol.* **2008**, 26, 620−625.

(8) Blanke, C. D.; Rankin, C.; Demetri, G. D.; Ryan, C. W.; von Mehren, M.; Benjamin, R. S.; Raymond, A. K.; Bramwell, V. H.; Baker, L. H.; Maki, R. G.; Tanaka, M.; Hecht, J. R.; Heinrich, M. C.; Fletche,r C. D.; Crowley, J. J.; Borden, E. C. Phase III randomized, intergroup trial assessing immatinib mesylate at two dose levels in patients with unresectable or metastatic gastrointestinal stromal tumors expressing the kit receptor tyrosine kinase:S0033. *J. Clin. Oncol.* **2008**, *26*, 626−632.

(9) Gounder, M. M.; Maki, R. G. Molecular basis for primary and secondary tyrosine kinase inhibitor resistance in gastrointestinal stromal tumor. *Cancer Chemother. Pharmacol.* **2011**, *67* (suppl 1), S25−S43.

(10) Corless, C. L.; Barnett, C. M.; Heinrich, M. C. Gastrointestinal stromal tumours: origin and molecular oncology. *Nat. Rev. Cancer* **2011**, *11*, 865−878.

(11) Call, J.; Walentas, C. D.; Eickhoff, J. C.; Scherzer, N. Survival of gastrointestinal stromal tumor patients in the imatinib era: life raft group observational registry. *BMC Cancer* **2012**, *12*, 90.

(12) Heinrich, M. C.; Owzar, K.; Corless, C. L.; Hollis, D.; Borden, E. C.; Fletcher, C. D.;

Ryan, C. W; von Mehren, M.; Blanke, C. D.; Rankin, C.; Benjamin, R. S.; Bramwell, V. H.; Demetri, G. D.; Bertagnolli, M. M.; Fletcher, J. A. Correlation of kinase genotype and clinical outcome in the North American Intergroup Phase III Trial of imatinib mesylate for treatment of advanced gastrointestinal stromal tumor: GALGB 150105 study by cancer and Leukemia Group B and Southwest Oncology Group. *J. Clin. Oncol.* **2008**, *26*, 5360−5367.

(13) Heinrich, M. C.; Corless, C. L.; Demetri, G. D.; Blanke, C. D.; von Mehren, M.; Joensuu, H.; McGreevey, L. S.; Chen, C. J.; Van den Abbeele, A. D.; Druker, B. J.; Kiese, B.; Eisenberg, B.; Roberts, P. J.; Singer, S.; Fletcher, C. D.; Silberman, S.; Dimitrijevic, S.; Fletcher, J. A. Kinase mutations and imatinib response in patients with metastatic gastrointestinal stromal tumor. *J. Clin. Oncol.* **2003**, *21*, 4342−4349.

(14) Gastrointestinal Stromal Tumor Meta-Analysis Group (MetaGIST). Comparison of two doses of imatinib for the treatment of unresectable or metastatic gastrointestinal stromal tumors: a meta-analysis of 1640 patients. *J. Clin. Oncol.* **2010**, *28*, 1247−1253.

(15) Antonescu, C. R.; Besmer, P.; Guo, T.; Arkun, K.; Hom, G.; Koryotowski, B.; Leversha, M. A.; Jeffrey, P. D.; Desantis, D.; Singer, S.; Brennan, M. F.; Maki, R. G.; DeMatteo, R. P. Acquired resistance to imatinib in gastrointestinal stromal tumor occurs through secondary gene mutation. *Clin. Cancer Res.* **2005**, *11*, 182−4190.

(16) Heinrich, M. C.; Maki, R. G.; Corless, C. L.; Antonescu, C. R.; Harlow, A.; Griffith, D.; Town, A.; McKinley, A.; Ou, W. B.; Fletcher, J. A.; Fletcher, C. D.; Huang, X.; Cohen, D.

P.; Baum, C. M.; Demetri, G. D. Primary and secondary kinase genotypes correlate with the biological and clinical activity of sunitinib in imatinib-resistant gastrointestinal stromal tumor. *J. Clin. Oncol.* **2008**, *26*, 5352−5359.

(17) Demetri, G. D.; van Oosterom, A. T.; Garrett, C. R.; Blackstein, M. E.; Shah, M. H.; Verweij, J.; McArthur, G.; Judson, I. R.; Heinrich, M. C.; Morgan, J. A.; Desai, J.; Fletcher, C. D.; George, S.; Bello, C. L.; Huang, X.; Baum, C. M.; Casali, P. G. Efficacy and safety of sunitinib in patients with advanced gastrointestinal stromal tumour after failure of imatinib: a randomised controlled trial. *Lancet* **2006**, *368*, 1329−1338.

(18) Demetri, G. D.; Reichardt, P.; Kang, Y. K.; Blay, J. Y.; Rutkowski, P.; Gelderblom, H.; Hohenberger, P.; Leahy, M.; von Mehren, M.; Joensuu, H.; Badalamenti, G.; Blackstein, M.; Le Cesne, A.; Schöffski, P.; Maki, R. G.; Bauer, S.; Nguyen, B. B.; Xu, J.; Nishida, T,; Chung, J.; Kappeler. C.; Kuss, I.; Laurent, D.; Casali, P. G. Efficacy and safety of regorafenib for advanced gastrointestinal stromal tumours after failure of imatinib and sunitinib (GRID): an international, multicentre, randomised, placebo-controlled, phase 3 trial. *Lancet* **2013**, *381*, 295−302.

(19) Tallman, M. S.; Gilliland, D. G.; Rowe, J. M. Drug therapy for acute myeloid leukemia. *Blood* **2005**, *106*, 1154−1163.

(20) Gilliland, D. G.; Griffin, J. D. The roles of FLT3 in hematopoiesis and leukemia. *Blood* **2002**, *100*, 1532−1542.

(21) Stirewalt, D. L.; Radich, J. P. The role of FLT3 in haematopoietic malignancies. *Nat.*

Rev. Cancer **2003**, *3*, 650−665.

(22) Fröhling, S.; Schlenk, R. F.; Breitruck, J.; Benner, A.; Kreitmeier, S.; Tobis, K.; Döhner, H.; Döhner, K. Prognostic significance of activating FLT3 mutations in younger adults (16 to 60 years) with acute myeloid leukemia and normal cytogenetics: a study of the AML Study Group Ulm. *Blood* **2002**, *100*, 4372−4380.

(23) Kikushige, Y.; Yoshimoto, G.; Miyamoto, T.; Iino, T.; Mori, Y.; Iwasaki, H.; Niiro, H.; Takenaka, K.; Nagafuji, K.; Harada, M.; Ishikawa, F.; Akashi, K. Human Flt3 is expressed at the hematopoietic stem cell and the granulocyte/macrophage progenitor stages to maintain cell survival. *J. Immunol.* **2008**, *180*, 7358−7367.

(24) Abu-Duhier, F. M.; Goodeve, A. C.; Wilson, G. A.; Care, R. S.; Peake, I. R.; Reilly, J. T. Identification of novel FLT-3 Asp835 mutations in adult acute myeloid leukaemia. *Br. J. Haematol.* **2001**, *113*, 983−988.

(25) Boissel, N.; Leroy, H.; Brethon, B.; Philippe, N.; de Botton, S.; Auvrignon, A.; Raffoux, E.; Leblanc, T.; Thomas, X.; Hermine, O.; Quesnel, B.; Baruchel, A.; Leverger, G.; Dombret, H.; Preudhomme, C. Incidence and prognostic impact of c-kit, FLT3, and Ras gene mutations in core binding factor acute myeloid leukemia (CBF-AML). *Leukemia* **2006**, *20*, 965−970.

(26) Beghini, A.; Ripamonti, C. B.; Cairoli, R.; Cazzaniga, G.; Colapietro, P.; Elice, F.; Nadali, G,; Grillo, G.; Haas, O. A.; Biondi, A.; Morra, E.; Larizza, L. KIT activating mutations: incidence in adult and pediatric acute myeloid leukemia, and identification of

an internal tandem duplication. *Haematologica* **2004**, *89*, 920−925.

(27) Shen, Y.; Zhu, Y. M.; Fan, X.; Shi, J. Y.; Wang, Q. R.; Yan, X. J.; Gu, Z. H.; Wang, Y. Y.; Chen B.; Jiang, C. L.; Yan, H.; Chen, F. F.; Chen, H. M.; Chen, Z.; Jin, J.; Chen, S. J. Gene mutations patterns and their prognostic impact in a cohort of 1185 patients with acute myeloid leukemia. *Blood* **2011**, *118*, 5593−5603.

(28) Cairoli, R.; Beghini, A.; Grillo G.; Nadali, G.; Elice, F.; Ripamonti, C. B.; Colapietro, P.; Nichelatti, M.; Pezzetti, L.; Lunghi, M.; Cuneo, A.; Viola, A.; Ferrara, F.; Lazzarino, M.; Rodeghiero, F.; Pizzolo, G.; Larizza, L.; Morra, E. Prognostic impact of c-KIT mutations in core binding factor leukemias and Italian retrospective study. *Blood* **2006**, *107*, 3463−3468.

(29) Kim, H. J.; Ahn, H. K.; Jung, C. W.; Moon, J. H.; Park, C. H.; Lee, K. O.; Kim, S. H.; Kim, Y. K.; Kim, H. J.; Sohn, S. K.; Kim, S. H.; Lee, W. S.; Kim, K. H.; Mun, Y. C.; Kim H.; Park, J.; Min, W. S.; Kim, H. J.; Kim, D. H. KIT D816 mutation associates with adverse outcomes in core binding factor acute myeloid leukemia, especially in the subgroup with RUNX1/RUNX1T1 rearrangement. *Ann. Hematol.* **2013**, *92*, 163−171.

(30) Chen, L. T.; Chen, C. T.; Jiaang, W. T.; Chen, T. Y.; Butterfield, J. H.; Shih, N. Y.; Hsu, J. T.; Lin, H. Y.; Lin, S. F.; Tsai, H. J. BPR1J373, an oral multiple tyrosine kinase inhibitor, targets c-KIT for the treatment of c-KIT−driven myeloid leukemia. *Mol. Cancer Ther.* **2016** *15*, 2323−2333.

(31) Zaker, F.; Mohammadzadeh, M.; Mohammadi, M. Detection of KIT and FLT3

mutations in acute myeloid leukemia with different subtypes. *Arch. Iran. Med.* **2010**, *13*, 21−25.

(32) Stone, R. M.; Mandrekar, S. J.; Sanford, B. L.; Laumann, K.; Geyer, S.; Bloomfield, C. D.; Thiede, C. 1.; Prior, T. W.; Döhner, K.; Marcucci, G.; Lo-Coco, F.; Klisovic, R. B.; Wei, A.; Sierra, J.; Sanz, M. A.; Brandwein, J. M.; de Witte, T.; Niederwieser, D.; Appelbaum F. R.; Medeiros, B. C.; Tallman, M. S.; Krauter, J.; Schlenk, R. F.; Ganser, A.; Serve, H.; Ehninger, G.; Amadori, S.; Larson, R. A.; Döhner, H. Midostaurin plus chemotherapy for acute myeloid leukemia with a FLT3 mutation. *N. Engl. J. Med.* **2017**, *77*, 454−464.

(33) Perl, A. E.; Martinelli, G.; Cortes, J. E.; Neubauer, A.; Berman, E.; Paolini, S.; Montesinos, P.; Baer, M. R.; Larson, R. A.; Ustun, C.; Fabbiano, F.; Erba, H. P.; Di Stasi, A.; Stuart, R.; Olin, R.; Kasner, M.; Ciceri, F.; Chou, W. C.; Podoltsev, N.; Recher, C.; Yokoyama, H.; Hosono, N.; Yoon, S. S.; Lee, J. H.; Pardee, T.; Fathi, A. T.; Liu, C.; Hasabou, N.; Liu, X.; Bahceci, E.; Levis, M. J. Gilteritinib or chemotherapy for relapsed or refractory FLT3-mutated AML. *N. Engl. J. Med.* **2019**, *381*, 1728−1740.

(34) Ashman, L. K.; Griffith, R. Therapeutic targeting of c-KIT in cancer. *Expert Opin. Investig. Drugs* **2013**, *22*, 103−115.

(35) Cammenga, J.; Bergholz, U.; Sommer, G.; Sommer, G.; Besmer, P.; Fiedler, W.; Stocking, C. Extracellular KIT receptor mutants, commonly found in core binding factor AML, are constitutively active and respond to imatinib mesylate. *Blood* **2005**, *106*,

3958-3961.

(36) Mpakou, V. E.; Kontsioti, F.; Papageorgiou, S.; Spathis, A.; Kottaridi, C.; Girkas, K.; Karakitsos, P,; Dimitriadis, G.; Dervenoulas, I.; Pappa, V. Dasatinib inhibits proliferation and induces apoptosis in the Kasumi-1 cell line bearing the t(8;21)(q22;q22) and the N822K c-kit mutation. *Leuk. Res.* **2013**, *37*, 175−182.

(37) Cairoli, R.; Beghini, A.; Morello, E.; Grillo, G.; Montillo, M.; Larizza, L.; Morra, E. Imatinib mesylate in the treatment of core binding factor leukemias with KIT mutations a report of three cases. *Leuk. Res.* **2005**, *29*, 397−400.

(38) Paschka, P.; Schlenk, R. F.; Weber, D.; Benner, A.; Bullinger, L.; Heuser, M.; Gaidzik, V. I.; Thol, F.; Agrawal, M.; Teleanu, V.; Lübbert, M.; Fiedler, W.; Radsak, M.; Krauter, J.; Horst, H. A.; Greil, R.; Mayer, K.; Kündgen, A.; Martens, U.; Heil, G.; Salih, H. R.; Hertenstein, B.; Schwänen, C.; Wulf, G.; Lange, E.; Pfreundschuh, M.; Ringhoffer, M.; Girschikofsky, M.; Heinicke, T.; Kraemer, D.; Göhring, G.; Ganser, A.; Döhner, K.; Döhner, H. Adding dasatinib to intensive treatment in core-binding factor acute myeloid leukemia-results of the AMLSG 11-08 trial. *Leukemia* **2018**, *32*, 1621−1630.

(39) Chen, C. T.; Hsu. J. T.; Lin, W. H.; Lu, C. T.; Yen, S. C.; Hsu, T.; Huang, Y. L.; Song, J. S.; Chen, C. H.; Chou, L. H.; Yen, K. J.; Chen, C. P.; Kuo, P. C.; Huan, C. L.; Liu, H. E.; Chao, Y. S.; Yeh, T. K.; Jiaang, W. T. Identification of a potent 5-phenyl-thiazol-2-ylamine-based inhibitor of FLT3 with activity against drug resistance-conferring point mutations. *Eur. J. Med. Chem.* **2015**, *100*, 151−161.

(40) Davis, M. I.; Hunt, J. P.; Herrgard, S.; Ciceri, P.; Wodicka, L. M.; Pallares, G.; Hocker, M.; Treiber, D. K.; Zarrinkar, P. P. Comprehensive analysis of kinase inhibitor selectivity. *Nat. Biotechnol*. **2011**, *29*, 1046−1051.

(41) Broekman, F.; Giovannetti, E.; Peters, G. J. Tyrosine kinase inhibitors: Multi-targeted or single-targeted? *World J. Clin. Oncol.* **2011**, *2*, 80−93.

(42) Bettati, M.; Churcher, I.; Hunt, P. A.; Steadman, V. A. Aminothiazole Derivatives as Inhibitors of MARK. PCT Patent WO 2007141571, December 13, 2007.

(43) Mjambili, F.; Njoroge, M.; Naran, K.; De Kock, C.; Smith, P. J.; Mizrahi, V.; Warner, D.; Chibale, K. Synthesis and biological evaluation of 2-aminothiazole derivatives as antimycobacterial and antiplasmodial agents. *Bioorg. Med. Chem. Lett.* **2014**, *24*, 560−564.

(44) Francini, C. M.; Fallacara, A. L.; Artusi, R.; Mennuni, L.; Calgani, A.; Angelucci, A.; Schenone, S.; Botta, M. Identification of aminoimidazole and aminothiazole derivatives as Src family kinase inhibitors. *ChemMedChem* **2015**, *10*, 2027−2041.

(45) Wu, T. S.; Lin, W. H; Tsai, H. J.; Hsueh, C. C.; Hsu, T.; Wang, P. C.; Lin, H. Y.; Peng, Y. H.; Lu, C. T.; Lee, L. C.; Tu, C. H.; Kung, F. C.; Shiao, H. Y.; Yeh, T. K.; Song, J. S.; Chang, J. Y.; Su, Y. C.; Chen, L. T.; Chen, C. T.; Jiaang, W. T.; Wu, S. Y. Discovery of conformational control inhibitors switching off the activated c-KIT and targeting a broad range of clinically relevant c-KIT mutants. *J. Med. Chem.* **2019**, *62*, 3940−3957.

(46) Lin, W. H.; Hsu, J. T.; Hsieh, S. Y.; Chen, C. T.; Song, J. S.; Yen, S. C.; Hsu, T.; Lu, C.

T.; Chen, C. H.; Chou, L. H.; Yang, Y. N.; Chiu, C. H.; Chen, C. P.; Tseng, Y. J.; Yen, K. J.; Yeh, C. F.; Chao, Y. S.; Yeh, T. K.; Jiaang, W. T. Discovery of 3-phenyl-1H-5-pyrazolylamine derivatives containing a urea pharmacophore as potent and efficacious inhibitors of FMS-like tyrosine kinase-3 (FLT3). *Bioorg. Med. Chem.* **2013**, *21*, 2856−2867.

(47) Tu, C. H.; Lin, W. H.; Peng, Y. H.; Hsu, T.; Wu, J. S.; Chang, C.Y.; Lu, C. T.; Lyu, P. C.; Shih, C.; Jiaang, W. T.; Wu, S. Y. Pyrazolylamine derivatives reveal the conformational switching between type I and type II binding modes of anaplastic lymphoma kinase (ALK). *J. Med. Chem.* **2016**, 59, 3906−3919.

(48) Heinrich, M. C.; Marino-Enriquez, A.; Presnell, A.; Donsky, R. S.; Griffith, D. J.; McKinley, A.; Patterson, J.; Taguchi, T.; Liang, C. W.; Fletcher, J. A. Sorafenib inhibits many kinase mutations associated with drug-resistant gastrointestinal stromal tumors. *Mol. Cancer Ther.* **2012**, *11*, 1770−1780.

Table of Contents Graphic

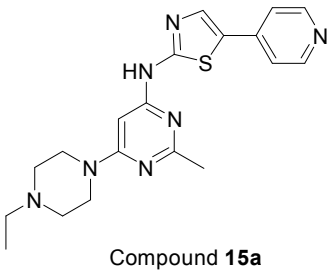

Compound **15a**

c-KIT and FLT3: IC_{50} < 100 nM
pc-KIT and pFLT3: IC_{50} < 100 nM
Mutant forms of c-KIT: IC_{50} < 100 nM
GIST cell lines GIST-T1, 882, 430 and 48: GI_{50} < 25 nM
AML cell lines MOLM-13, MV4;11 and kasumi-1: GI_{50} < 15 nM
Bioavailability: 36% (rats), 68% (mice)
In vivo xenograft models: GIST430 (regression, 30 mg/kg), two GIST PDX (TGI > 80%, 30 mg/kg), Kasumi-1 (regression, 20 and 30 mg/kg) and MOLM-13 (regression, 50 and 100 mg/kg)